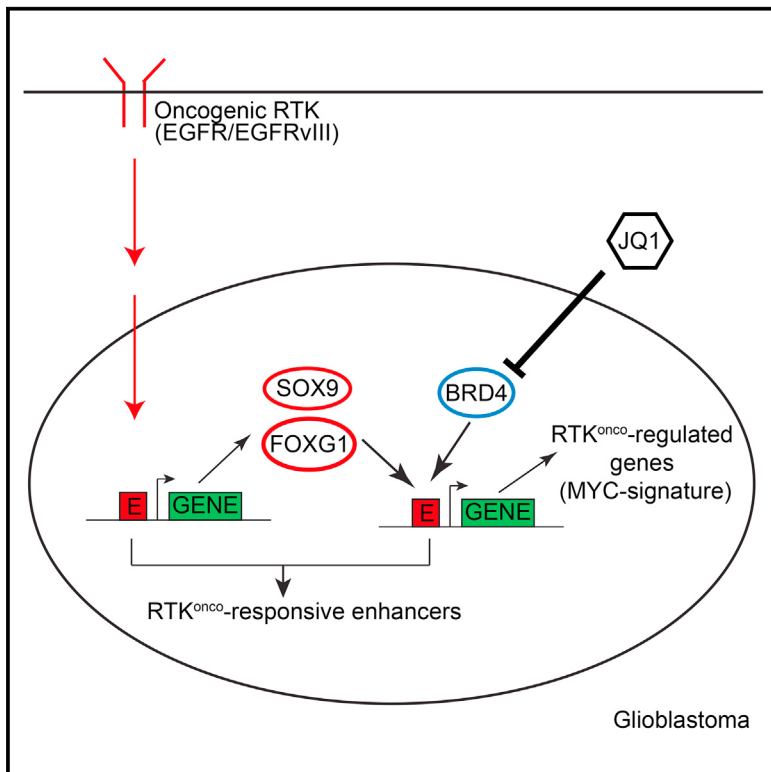


# Molecular Cell

## EGFR Mutation Promotes Glioblastoma through Epigenome and Transcription Factor Network Remodeling

### Graphical Abstract



### Authors

Feng Liu, Gary C. Hon,  
Genaro R. Villa, ...,  
Webster K. Cavenee, Bing Ren,  
Paul S. Mischel

### Correspondence

biren@ucsd.edu (B.R.),  
pmischel@ucsd.edu (P.S.M.)

### In Brief

Epidermal growth factor receptor (*EGFR*) gene amplification and mutations are the most common oncogenic events in glioblastoma (GBM). Through an integrative genomics analysis, Liu et al., identify a role for transcriptional/epigenetic remodeling in *EGFR*-dependent pathogenesis and suggest a mechanistic basis for epigenetic therapy.

### Highlights

- Oncogenic EGFRvIII mutation remodels the enhancer landscape in GBM
- EGFRvIII induces SOX9 and FOXG1 transcription in GBM
- SOX9 and FOXG1 collaborate to activate an oncogenic gene regulatory program
- EGFRvIII-dependent transcription sensitizes GBM cells to JQ1

### Accession Numbers

GSE72468

# EGFR Mutation Promotes Glioblastoma through Epigenome and Transcription Factor Network Remodeling

Feng Liu,<sup>1,11</sup> Gary C. Hon,<sup>1,10,11</sup> Genaro R. Villa,<sup>1,6</sup> Kristen M. Turner,<sup>1</sup> Shiro Ikegami,<sup>1</sup> Huijun Yang,<sup>1</sup> Zhen Ye,<sup>1</sup> Bin Li,<sup>1</sup> Samantha Kuan,<sup>1</sup> Ah Young Lee,<sup>1</sup> Ciro Zanca,<sup>1</sup> Bowen Wei,<sup>6</sup> Greg Lucey,<sup>6</sup> David Jenkins,<sup>1</sup> Wei Zhang,<sup>7</sup> Cathy L. Barr,<sup>8,9</sup> Frank B. Furnari,<sup>1,12</sup> Timothy F. Cloughesy,<sup>6</sup> William H. Yong,<sup>6</sup> Timothy C. Gahman,<sup>1</sup> Andrew K. Shiau,<sup>1</sup> Webster K. Cavenee,<sup>1,3,5</sup> Bing Ren,<sup>1,4,5,\*</sup> and Paul S. Mischel<sup>1,2,5,\*</sup>

<sup>1</sup>Ludwig Institute for Cancer Research, La Jolla, CA 92093, USA

<sup>2</sup>Department of Pathology, UCSD School of Medicine, La Jolla, CA 92093, USA

<sup>3</sup>Department of Medicine, UCSD School of Medicine, La Jolla, CA 92093, USA

<sup>4</sup>Department of Cellular and Molecular Medicine, Institute of Genomic Medicine, UCSD School of Medicine, La Jolla, CA 92093, USA

<sup>5</sup>Moores Cancer Center, UCSD School of Medicine, La Jolla, CA 92093, USA

<sup>6</sup>David Geffen UCLA School of Medicine, Los Angeles, CA 90095, USA

<sup>7</sup>Department of Pathology, University of Texas MD Anderson Cancer Center, Houston, TX 77030, USA

<sup>8</sup>Toronto Western Research Institute, University Health Network, Toronto, ON M5T 2S8, Canada

<sup>9</sup>Program in Neurosciences and Mental Health, Hospital for Sick Children, Toronto, ON M5T 2S8, Canada

<sup>10</sup>Present address: Cecil H. and Ida Green Center for Reproductive Biology Sciences and Division of Basic Reproductive Biology Research, Department of Obstetrics and Gynecology, University of Texas Southwestern Medical Center, Dallas, TX 75390, USA

<sup>11</sup>Co-first author

\*Correspondence: biren@ucsd.edu (B.R.), pmischel@ucsd.edu (P.S.M.)

<http://dx.doi.org/10.1016/j.molcel.2015.09.002>

## SUMMARY

Epidermal growth factor receptor (EGFR) gene amplification and mutations are the most common oncogenic events in glioblastoma (GBM), but the mechanisms by which they promote aggressive tumor growth are not well understood. Here, through integrated epigenome and transcriptome analyses of cell lines, genotyped clinical samples, and TCGA data, we show that EGFR mutations remodel the activated enhancer landscape of GBM, promoting tumorigenesis through a SOX9 and FOXG1-dependent transcriptional regulatory network *in vitro* and *in vivo*. The most common EGFR mutation, EGFRvIII, sensitizes GBM cells to the BET-bromodomain inhibitor JQ1 in a SOX9, FOXG1-dependent manner. These results identify the role of transcriptional/epigenetic remodeling in EGFR-dependent pathogenesis and suggest a mechanistic basis for epigenetic therapy.

## INTRODUCTION

Growth factor receptors are frequently amplified and/or mutated in cancer (Ciriello et al., 2013; Kandoth et al., 2013; Vogelstein et al., 2013). Growth factor receptor mutations activate intracellular signaling cascades that promote growth, at least in part, by regulating transcriptional networks (Lee and Young, 2013). Master transcription factors (TFs) interact with *cis*-regulatory DNA sequences to control transcriptional repertoires that drive tumor growth and survival (Baylin and Jones, 2011; Suvà et al., 2013).

However, the mechanisms by which mutated growth factor receptors control the transcriptional machinery and alter the epigenetic landscape of cancer cells to reprogram transcription are not well understood.

Glioblastoma (GBM) is the most common primary brain cancer of adults and one of the most lethal of all human malignancies (Cloughesy et al., 2014). The epidermal growth factor receptor (EGFR) is amplified and/or mutated in up to 60% of GBMs, promoting tumor growth and survival through persistent activation of signaling networks and metabolic reprogramming (Cloughesy et al., 2014; Furnari et al., 2015). Currently, the impact of EGFR alteration on the transcriptional/epigenetic landscape of tumor cells is not known. Here, using global RNA-sequencing (seq) and chromatin immunoprecipitation (ChIP)-seq analysis of GBM cell lines, patient-derived tumor cells in neurosphere culture and clinical biopsies genotyped for EGFR mutation status, we identify a SOX9 and FOXG1-dependent transcriptional regulatory network that remodels the enhancer activation landscape to drive EGFRvIII-dependent tumorigenesis *in vitro* and *in vivo* and sensitizes GBM cells to the bromodomain and extra-terminal (BET)-bromodomain inhibitor JQ1. These results link oncogene-induced signaling with a highly specific program of epigenetic remodeling, suggesting that global epigenetic analysis of specific oncogene mutations may provide new therapeutic insights.

## RESULTS

### Integrative Analyses of Chromatin Landscape Induced by EGFRvIII

We analyzed histone H3 lysine 4 monomethylation (H3K4me1) and histone H3 lysine 27 acetylation (H3K27ac)—two histone modifications associated with poised and active enhancers

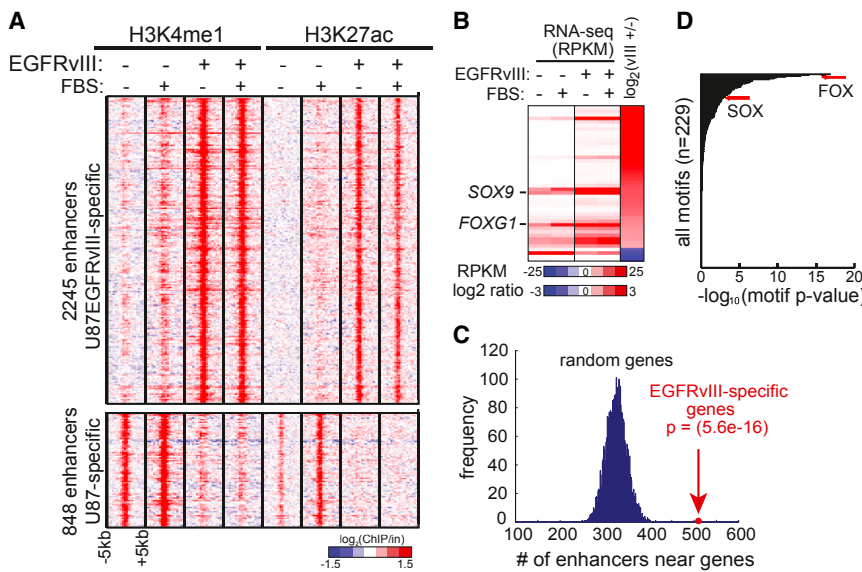


**Figure 1. Integrative Analyses of Chromatin and Transcriptional Landscape Induced by Hyperactivated EGFR in GBM**

(A) Heat map of ChIP-seq experiments using antibodies against H3K4me1 and H3K27ac in U87 and U87EGFRvIII cells. The presence of EGFRvIII results in the activation and silencing of distinct sets of enhancers. Note that these potential enhancers show little response to 10% fetal bovine serum (FBS), which contains various growth factors.

(B) Heat map of RNA-seq data shows the transcript levels of TF genes differentially expressed between U87 and U87EGFRvIII cells (see also Figure S1).

(C) The number of EGFRvIII-responsive enhancers near random gene sets (blue), as compared to a set of EGFRvIII-specific genes (red).

(D) Enrichment scores for known transcription factor motifs at EGFRvIII-responsive enhancers. FOX and SOX motifs are indicated. See also Figure S1 and Table S4.

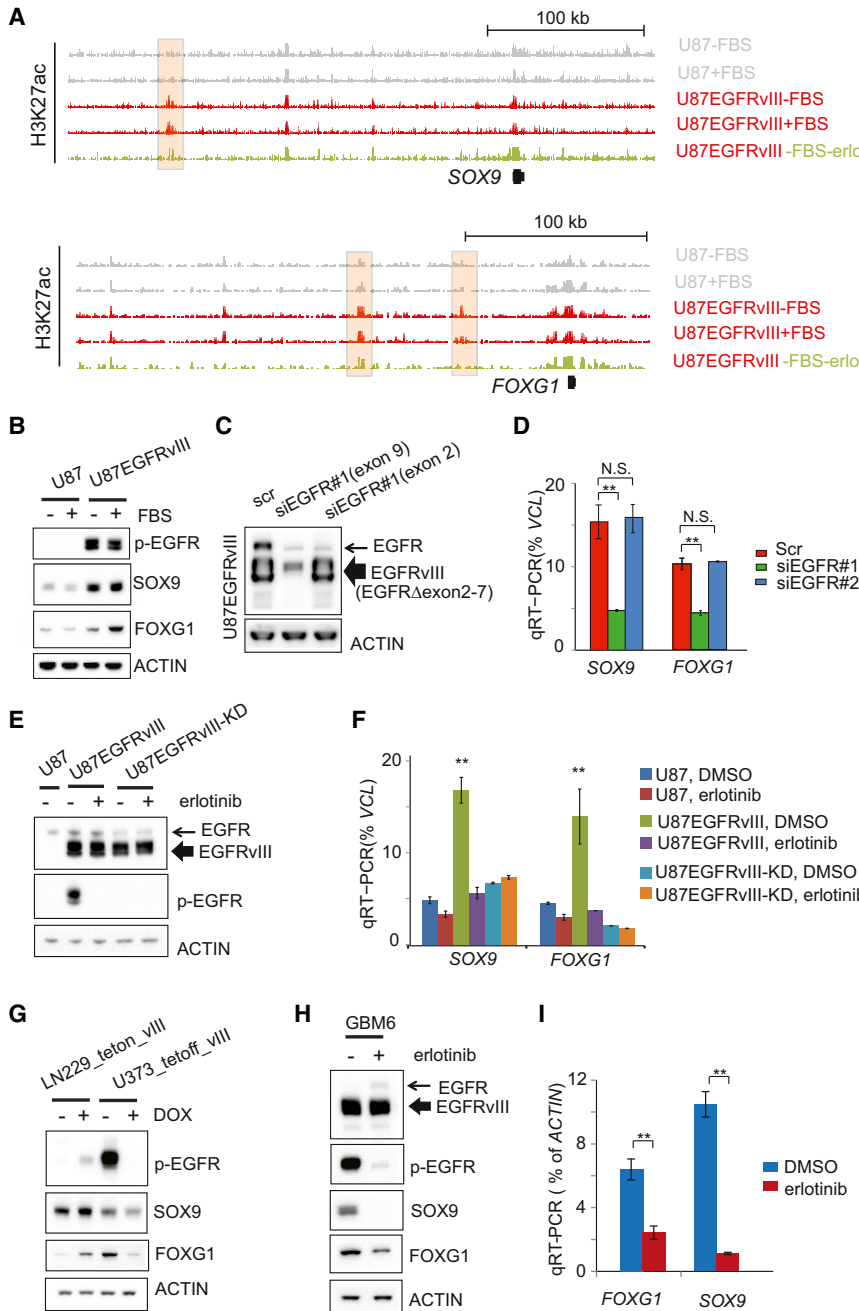
(Creighton et al., 2010; Heintzman et al., 2007; Rada-Iglesias et al., 2011)—by ChIP-seq in isogenic U87 GBM cells with, or without, stable expression of the ligand-independent activated EGFR mutation, EGFRvIII. This analysis revealed 2,245 putative enhancers that were specifically activated in EGFRvIII-expressing GBM cells (Figure 1A). The activation state of these enhancers was not changed by the addition of serum, which contained growth factors that could activate other cell surface receptors (Figure 1A).

To gain insight into the regulation of EGFRvIII-specific transcription that might be regulated by these putative enhancers, we performed RNA-seq (Figure 1B). The EGFRvIII-activated enhancers identified by H3K4me1 and H3K27ac ChIP-seq were significantly enriched near EGFRvIII-upregulated transcripts, suggesting the presence of a coordinated, EGFRvIII-regulated, transcriptional network (Figure 1C). Analysis of TF recognition motifs within EGFRvIII-activated enhancers showed that binding sites for many of the 41 TFs upregulated in EGFRvIII-expressing GBM cells were highly enriched (Figure S1A). In particular, motifs for the FOX and SOX family of TFs were among the most highly enriched motifs (Figure 1D). SOX9 and FOXG1 transcripts, which have been implicated in brain development and are thought to play a role in cancer (Guo et al., 2012; Rani et al., 2013; Seoane et al., 2004; Swartling et al., 2012; Verginelli et al., 2013; Wang et al., 2012), were both highly elevated by EGFRvIII expression (Figure 1B). Therefore, we set out to determine whether EGFRvIII regulates SOX9 and FOXG1 expression and to study its functional importance.

### EGFRvIII Activates the Transcription of SOX9 and FOXG1

In GBM cells treated with the EGFR tyrosine kinase inhibitor erlotinib, we detected a marked decrease in H3K27ac at putative enhancers near SOX9 and FOXG1 (Figure 2A). The erlotinib-sensitive H3K27ac peak near FOXG1 forms long-range chromatin looping with the FOXG1 promoter, as evidenced by a circularized chromosome confirmation capture (4C-seq) experiment, supporting its role as a FOXG1 enhancer (Figure S2A). We examined

the effect of EGFRvIII on SOX9 and FOXG1 mRNA and protein levels in multiple GBM cell line contexts. In U87 GBM cells, EGFRvIII expression dramatically increased SOX9 and FOXG1 transcript and protein levels (Figures 1B and 2B), which was inhibited by erlotinib (Figure S2B). The mTOR kinase inhibitor torin1 and the MEK inhibitor U0126 also reduced SOX9 and FOXG1 levels, suggesting that EGFRvIII controls expression of these TFs through downstream signaling (Figures S2B and S2C). To determine whether wild-type EGFR and mutant EGFR, EGFRvIII, differentially regulate SOX9 and FOXG1, we generated a small interfering (si)RNA construct targeting exon 9 of EGFR, which knocks down both wild-type EGFR and EGFRvIII, and an siRNA construct targeting exon 2, a region deleted in EGFRvIII, which only knocks down wild-type EGFR expression (Figure 2C). As shown in Figure 2D, knockdown of EGFRvIII, but not wild-type EGFR alone, resulted in significantly reduced SOX9 and FOXG1 transcript levels. To test whether EGFRvIII's effect on SOX9 and FOXG1 depended on its kinase activity, we introduced a kinase dead EGFRvIII construct (EGFRvIII-KD; Figure 2E) (Akhavan et al., 2013; Huang et al., 1997). In U87 GBM cells, EGFRvIII, but not kinase dead EGFRvIII, significantly elevated SOX9 and FOXG1 transcript levels in an erlotinib-sensitive fashion (Figure 2F), indicating that: (1) the observed effect of EGFRvIII on SOX9 and FOXG1 transcription was not due to exogenous EGFRvIII expression, and (2) the effect of EGFRvIII on SOX9 and FOXG1 expression was dependent on EGFRvIII kinase activity. To confirm the effect of EGFRvIII in different GBM cell line contexts, we expressed EGFRvIII under the control of a doxycycline inducible promoter in LN229 GBM cells and expressed EGFRvIII under the control of a doxycycline repressible promoter in U373 GBM cells. EGFRvIII potently upregulated SOX9 and FOXG1 protein expression in both cell lines (Figure 2G). To determine whether endogenously expressed EGFRvIII similarly regulates SOX9 and FOXG1, we analyzed GBM6 patient-derived cells in neurosphere culture (Nathanson et al., 2014; Sarkaria et al., 2007). Erlotinib treatment greatly reduced SOX9 and FOXG1 protein expression in GBM6 cells, demonstrating that endogenously expressed



EGFRvIII also regulates SOX9 and FOXG1 through its kinase activity in a non-engineered cell context (Figures 2H and 2I).

### SOX9 and FOXG1 Interact with EGFRvIII-Responsive Enhancers

To determine whether SOX9 and FOXG1 bind to EGFRvIII-responsive enhancers, we performed ChIP-quantitative (q) PCR on two informative genes, *FOXF1* and *TFAP2c*, using antibodies directed against SOX9 and FOXG1. We focused on these two genes because: (1) they are near EGFRvIII-responsive enhancers (defined by H3K27Ac and H3K4me1, being

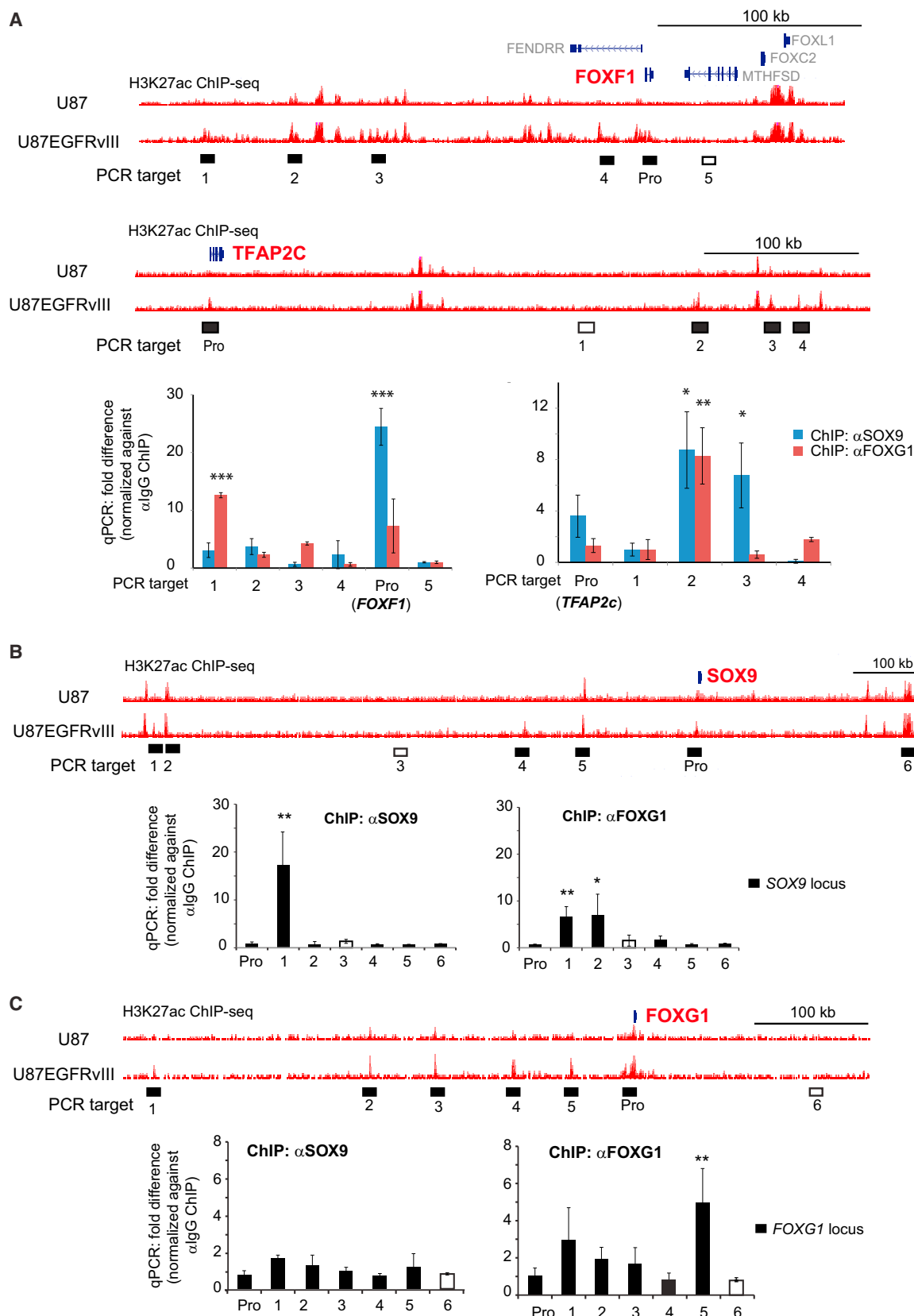
**Figure 2. EGFRvIII Activates the Transcription of SOX9 and FOXG1**

- (A) Snapshots of UCSC genome browser of ChIP-seq experiments at the loci of *SOX9* and *FOGX1*. The shaded H3K27ac peaks indicated putative EGFRvIII-responsive enhancers.
- (B) Western blots of U87 and U87EGFRvIII cells cultured with or without FBS. The SOX9 and FOXG1 protein levels are at much higher levels in U87EGFRvIII cells.
- (C) Western blots of U87EGFRvIII cells treated by siRNAs. A siRNA (siEGFR#1 targeting exon 9) knocks down the expression of both wild-type EGFR and EGFRvIII; the other siRNA (siEGFR#2 targeting exon 2) only knocks down wild-type EGFR (exons 2–7 are deleted in EGFRvIII).
- (D) qRT-PCR experiments show that siEGFR#1, but not siEGFR#2, is able to decrease the transcript levels of SOX9 and FOXG1.
- (E) Western blots show the expression of EGFRvIII and kinase dead EGFRvIII (EGFRvIII-KD). The erlotinib treatment (10  $\mu$ M for 24 hr) abrogates the kinase activity of EGFRvIII.
- (F) qRT-PCR of cells treated with erlotinib (\*\*p < 0.01 and t test). The error bars represent SD.
- (G) EGFRvIII regulates the expression of SOX9 and FOXG1 in the LN229\_teton\_vIII cell line, in which EGFRvIII is induced by doxycycline (DOX), and in U373\_tetoff\_vIII cell line, in which EGFRvIII is suppressed by DOX.
- (H and I) Erlotinib suppresses the expression of SOX9 and FOXG1 in a patient derived neurosphere GBM cell line, GBM6, which endogenously expresses EGFRvIII (\*\*p < 0.01 and t test). The error bars represent SD. See also Figure S2 and Table S3.

very high at enhancers near these genes in U87EGFRvIII cells and silent in U87 cells), (2) their expression was greatly elevated by the expression of EGFRvIII, and (3) SOX9 or FOXG1 knockdown abrogated their mRNA expression. As shown in Figure 3A, SOX9 and FOXG1 both bind to EGFRvIII-responsive enhancers near these two EGFR-regulated genes. Furthermore, we performed ChIP-qPCR on the *SOX9* and *FOGX1* loci, demonstrating that SOX9 and FOXG1 both bind to enhancers that may regulate them, thus providing compelling evidence for autoregulation (Figures 3B and 3C). Careful inspection of the ChIP-qPCR data suggested that FOXG1 might also cross regulate SOX9. FOXG1 knockdown reduced SOX9 transcript and protein levels, and vice versa, raising the possibility of a more complex form of cross regulation (Figures S3A and S3B).

### SOX9 and FOXG1 Correlate with EGFR Amplification/Mutation in Clinical GBM Samples

Having demonstrated that EGFRvIII controls SOX9 and FOXG1 expression in relatively simplified isogenic GBM cell culture



(legend on next page)

systems, we next examined the correlation between *EGFR*/EGFR<sub>vIII</sub> and SOX9/FOXG1 expression in a large cohort of clinical GBM samples in The Cancer Genome Atlas (TCGA) consortium (<http://cancergenome.nih.gov/>), consisting of gene expression microarray data from 598 GBMs (Brennan et al., 2013). Among the relatively large HMG/SOX and FOX TF families, the expression of SOX9 and FOXG1 were the most highly correlated with that of *EGFR* ( $p$  value/*FOXG1* =  $1.27 \times 10^{-18}$ ;  $p$  value/*SOX9* =  $1.10 \times 10^{-41}$ , Matlab correlation function; Figures 4A, S4A, and S4B). In a separate TCGA data set using RNA-seq profiles from 169 GBM tumor samples (Brennan et al., 2013), SOX9 and FOXG1 expression were significantly elevated in those GBMs bearing *EGFR* amplification and mutations, including EGFR<sub>vIII</sub> ( $p_{\text{FOXG1}} < 0.0038$ ;  $p_{\text{SOX9}} < 0.0017$ , Wilcoxon; Figures 4B and S4D).

A random forest classifier demonstrated that genetic alteration of growth factor receptors accurately predicted the levels of SOX9 (area under curve [AUC] = 0.94,  $p = 2.3 \times 10^{-15}$ , Z test) and FOXG1 (AUC = 0.83,  $p < 1 \times 10^{-15}$ , Z test), in GBM clinical samples driven largely by genetic alterations of *EGFR* (Figures 4C, S4E, and S4F). Furthermore, FGFR3 overexpression, which is associated with gene amplification and/or mutation (Parker et al., 2013; Singh et al., 2012), was associated with elevated SOX9 levels in the TCGA clinical GBM samples. Ligand-induced FGFR3 activation increased SOX9 levels in vitro (Figures S4E and S4G). Taken together with the mechanistic data showing that EGFR<sub>vIII</sub> promotes SOX9 and FOXG1 (Figure 2), these results indicate a strong association between *EGFR* genetic alterations and SOX9 and FOXG1 expression, as well as an association between FGFR3 and SOX9, in GBM. This association was also confirmed at the protein level. An immunohistochemical analysis of GBM tissue microarrays demonstrated significant correlations between phospho-EGFR, SOX9, and FOXG1 proteins, all of which were correlated with each other and with tumor cell proliferation rate, as measured by Ki67 staining (Figures 4G–4I). Analysis of TCGA data from other tumor types also demonstrated elevated SOX9 and FOXG1 in association with amplification of various growth factor receptors in a variety of cancers (Figures S4H and S4I; Table S1), suggesting that SOX9 and FOXG1 may be common transcriptional effectors downstream of growth factor alterations in multiple cancer types.

To further verify if the growth factor induced transcriptional program and epigenetic remodeling identified in the above cell models is present in GBM tumors, we performed ChIP-seq to profile the H3K4me1 and H3K27ac status of regulatory DNA sequences in a set of GBM clinical samples. There were 14 frozen GBM tissue samples that were screened for quality and six were selected based upon the presence of greater than 70% tumor cells in the tissue sample (Table S2). This included four GBMs with *EGFR* amplification and EGFR<sub>vIII</sub> mutation and two GBMs

with elevated FGFR3 transcript expression (Figure S4J). We also performed H3K4me1 and H3K27ac ChIP-seq on one low grade glioma bearing no receptor tyrosine kinase (RTK) mutations, but containing an IDH1 R132H mutation (Table S2). As a basis of comparison, we obtained H3K27ac ChIP-seq profiles from six different normal brain regions. There were two distinct clusters of growth factor-associated enhancers that were detected in the GBMs, which were not found in either the IDH1 mutant low grade glioma or in the normal brain samples (Figure 4D). These putative EGFR/FGFR3-activated enhancers were significantly enriched for binding sequence motifs of the SOX and FOX family of TFs (Figure 4E) and are located near genes differentially expressed between EGFR<sub>vIII</sub><sup>+</sup> and EGFR<sup>euploid</sup> GBMs (Figure 4F). Taken together, these results indicate the presence of a coordinated transcriptional program with epigenetic remodeling downstream of RTK genetic alterations in clinical GBM samples.

### SOX9 and FOXG1 Promote GBM In Vitro and In Vivo

To determine the functional role of SOX9 and FOXG1 in EGFR<sub>vIII</sub>-dependent tumor growth, we generated GBM cells stably expressing short hairpin (sh)RNAs targeting SOX9 and FOXG1 and performed ChIP-seq analysis to determine the effect of these knockdowns on the activation state of EGFR<sub>vIII</sub>-responsive enhancers. Knock down of either TF significantly decreased H3K27 acetylation and H3K4 monomethylation of EGFR<sub>vIII</sub>-responsive enhancers (Figures 5A and 5B). Further, knock down of either SOX9 or FOXG1 severely impaired the growth of U87EGFR<sub>vIII</sub> cells in culture and almost completely blocked colony formation in soft agar (Figures 5C and S5A–S5C). In vivo, SOX9 or FOXG1 knockdown resulted in a marked delay in tumor development along with significant reductions in tumor sizes in mice bearing SOX9 or FOXG1-knockdown tumors and this was associated with significantly longer survival (Figures 5D–5F and S5D–S5L).

To identify the global transcriptional repertoires controlled by SOX9 and FOXG1, we performed RNA-seq analysis of U87EGFR<sub>vIII</sub> cells with or without shRNA knock down of SOX9 or FOXG1. This analysis identified 993 and 1,920 genes whose expression was markedly reduced by SOX9 and FOXG1 knockdown, respectively, including 376 genes that are regulated by both TFs (Figure 5G). These 376 genes were highly overrepresented in gene ontologies that are associated with glioma and other cancer types, indicating a potentially important oncogenic function (Figure 5H). Taken together, these results indicate that SOX9 and FOXG1 collaborate to control a subset of EGFR<sub>vIII</sub>-regulated genes in GBM.

To identify actionable transcriptional programs regulated by SOX9 or FOXG1, we performed gene set enrichment analysis (GSEA) on the transcriptomes of SOX9/FOXG1 knockdown cells. This analysis indicated significant enrichment for

### Figure 3. SOX9 and FOXG1 Interact with EGFR<sub>vIII</sub>-Responsive Enhancers

(A) UCSC genome browser snapshots are shown at the top. ChIP-qPCR was used to detect the binding of SOX9 and FOXG1 with putative EGFR<sub>vIII</sub>-responsive enhancer elements (H3K27ac high in U87EGFR<sub>vIII</sub>/low in U87) near *FOXF1* and *TFAP2c*, both of which are induced by EGFR<sub>vIII</sub> in U87 cells (Figure S1A). The PCR targets are shown as filled blocks below corresponding enhancer elements; control PCR target is shown as empty block (promoter: Pro). qPCR experiments are shown at the bottom.

(B) SOX9 and FOXG1 ChIP-qPCR at the SOX9 locus.

(C) SOX9 and FOXG1 ChIP-qPCR at the FOXG1 locus (\* $p < 0.05$ , \*\* $p < 0.01$ , \*\*\* $p < 0.001$ , and t test). The error bars represent SD. See also Figure S3 and Table S3.

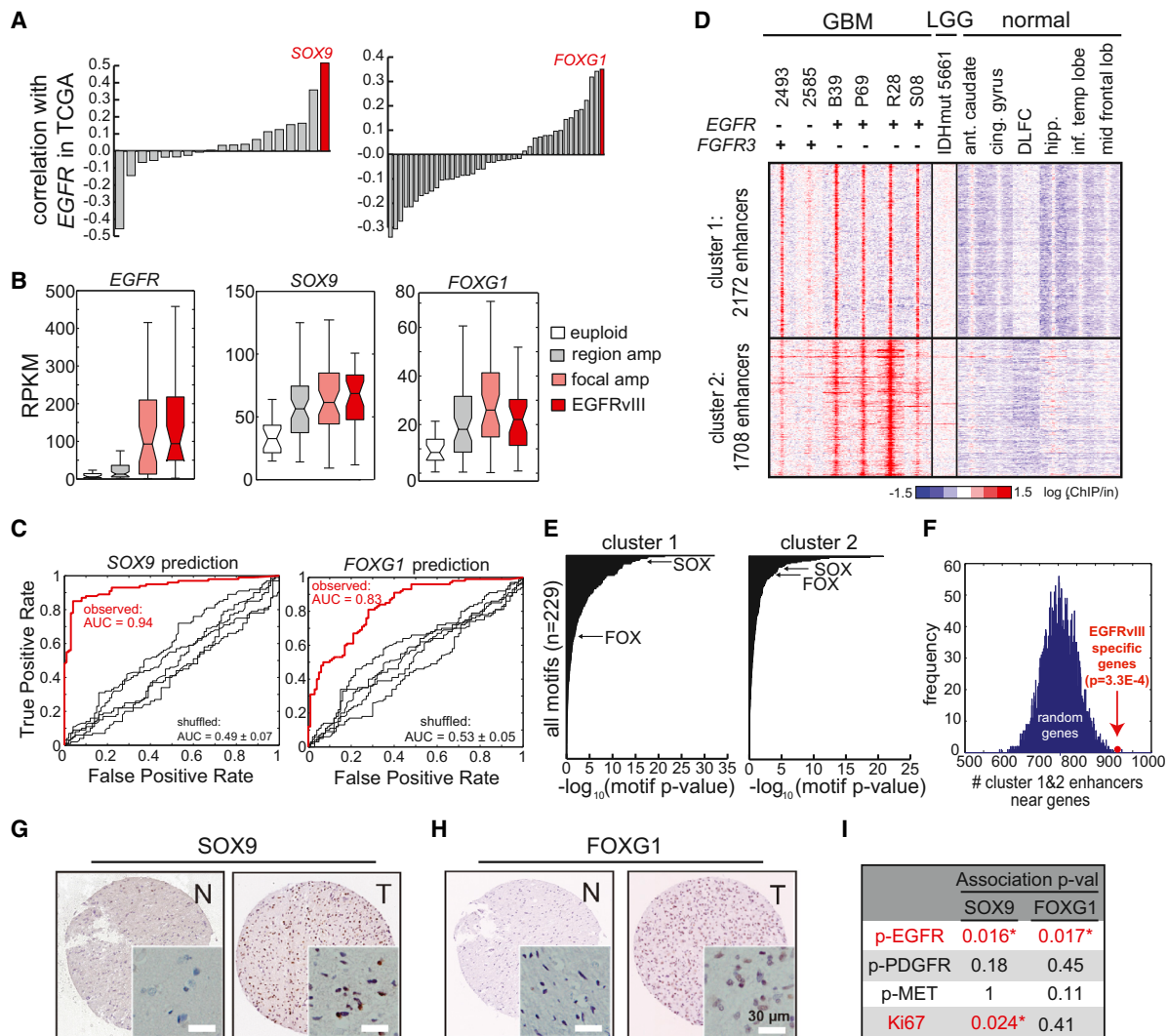


**Figure 4. SOX9 and FOXG1 Correlate with EGFR Amplification/Mutation in Clinical GBM Samples**

- (A) Correlation of the transcript levels of SOX and FOX families with EGFR in 598 tumors in the TCGA GBM microarray database. The SOX9 and FOXG1 show the highest correlation with EGFR among these two families.
- (B) Expression levels of EGFR, SOX9, and FOXG1 in TCGA GBM RNA-seq database. The SOX9 and FOXG1 are expressed at higher levels in tumors with EGFR amplification and mutation.
- (C) The levels of commonly amplified RTKs (Table S1) can accurately predict SOX9 and FOXG1 levels in GBM using a random forest classifier.
- (D) Heat map of ChIP-seq using tissue samples, including six GBMs (four expressing high levels of EGFR and two expressing high levels of FGFR3; Figure S4J), one low grade glioma (which carries IDH1 R132H mutation), and six normal brain tissues (Table S2). A comparison of H3K27ac peaks in these tissue samples revealed two clusters of enhancers that are active specifically in GBM with high levels of EGFR or FGFR3 (anterior caudate: ant.caudate; cingulate gyrus: cing.gyrus; dorsolateral prefrontal cortex: DLFC; hippocampus: hipp; inferior temporal lobe: inf.temp lobe; and middle frontal lobe: mid frontal lobe).
- (E) Putative enhancers active in high grade GBM are enriched with binding motifs HMG/SOX and FOX proteins.
- (F) GBM-specific enhancers are enriched near genes showing differential levels between EGFRvIII+ and EGFR euploid tumors in the TCGA GBM RNA-seq database.
- (G and H) Immunohistochemistry of tissue microarray containing normal and GBM tissue sections. The representative anti-SOX9 and anti-FOGX1 stains are shown (normal: N and tumor: T). The scale bar represents 30 µm.
- (I) Strong SOX9 and FOXG1 stains are significantly associated with high levels of phosphor-EGFR stain (marker of activated EGFR), while showing little correlation with phospho-PDGFR and phospho-MET. The statistics were performed using Fisher's exact test; one-tail p values are shown in the table. The asterisk indicates  $p < 0.05$ . See also Figure S4 and Tables S2 and S4.

previously identified c-MYC target genes and EGFR-regulated genes (Figure 5I), suggesting that SOX9 and FOXG1-coregulated genes play a role in promoting EGFR-dependent tumor cell growth.

### EGFRvIII Sensitizes GBM Cells to JQ1-Induced Cell Death through SOX9 and FOXG1

c-MYC expression, and transcription of its target genes, is regulated by BRD4, a BET protein family member, which acts as a

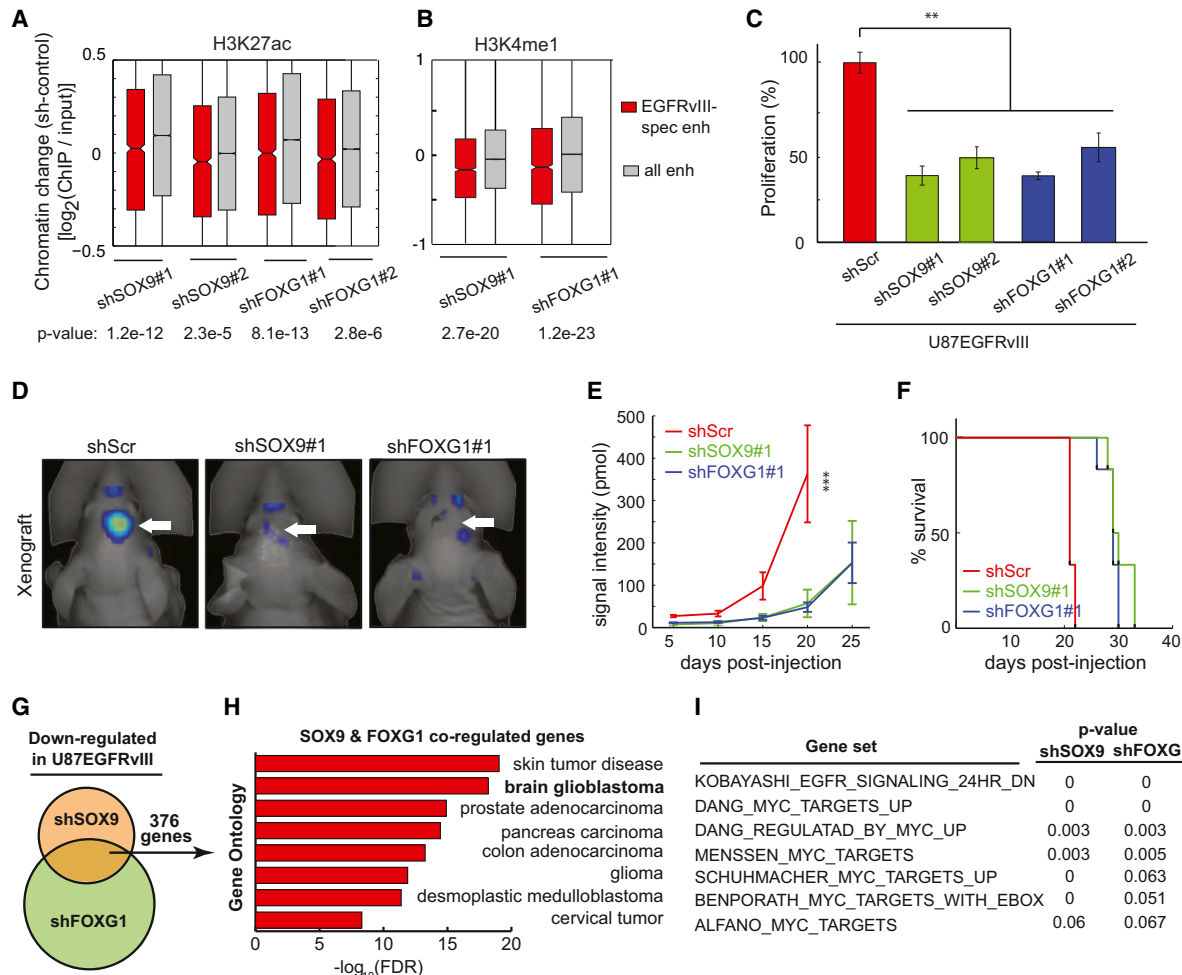


**Figure 5. SOX9 and FOXG1 Are Required for the Growth of EGFRvIII-Expressing GBM**

(A and B) ChIP-seq experiments indicate that SOX9 and FOXG1 knockdowns significantly decrease H3K27 acetylation and H3K4 monomethylation in the chromatin of EGFRvIII-responsive enhancers.

(C) Knock down of SOX9 or FOXG1 reduces the proliferation of U87EGFRvIII cells grown in petri dish (\*\*p < 0.01 and t test). The error bars represent SD.

(D) Fluorescence scan of an intracranial xenograft model of U87EGFRvIII cells transplanted into the mouse brain. The cells were engineered to constitutively express the near-infrared fluorescent protein iRFP720 so that tumor mass can be monitored by 3D fluorescence tomography. The white arrows indicate the sites where cancer cells were injected. Shown are representative images of the tumor scan at the 20<sup>th</sup> day post-injection.

(E) SOX9 or FOXG1 knock down slowed down the formation of tumors by U87EGFRvIII cells in vivo. At the 20<sup>th</sup> day post-injection, the fluorescence intensities of tumors formed by U87EGFRvIII<sup>shSOX9</sup> or U87EGFRvIII<sup>shFOXG1</sup> cells were significantly lower than those formed by U87EGFRvIII<sup>shScr</sup> cells (p value/shSOX9 ≤ 0.0001, p value/shFOXG1 ≤ 0.0001, t test, and n = 6 per group). The error bars represent SD.

(F) Kaplan-Meier survival curves of host mice for the xenograft experiments. The mice containing SOX9 or FOXG1 knockdown cells lived longer than the control mice (p value/shSOX9 ≤ 0.0001, p value/shFOXG1 ≤ 0.0001, and log-rank, Mantel-Cox, test).

(G) Venn diagram of the comparison of RNA-seq experiments using U87EGFRvIII, U87EGFRvIII<sup>shSOX9</sup>, and U87EGFRvIII<sup>shFOXG1</sup> cells. SOX9 and FOXG1 are both required for the expression of 397 genes in U87EGFRvIII.

(H) Gene ontology (GO) analysis indicates that SOX9 and FOXG1 co-regulated genes are associated with a variety of RTK-driven cancers.

(I) GSEA indicates that SOX9 and FOXG1 knockdowns led to the loss of gene signatures associated with the EGFR pathway and the proto-oncogenic c-MYC. See also Figure S5.

transcriptional cofactor (Shi and Vakoc, 2014). Notably, among the BET family members, *BRD4* transcript level was significantly correlated with that of SOX9 and FOXG1 in the TCGA database of GBMs (Figures 6A and 6B). *BRD4* transcription was also significantly increased in the classical GBM subtype that is enriched for EGFR-genetic alterations (Figure 6C). Consistent with earlier studies (Delmore et al., 2011; Filippakopoulos et al., 2010),

*BRD4* knock down or treatment with pan-BET bromodomain small molecule inhibitor JQ1 dramatically lowered c-MYC levels (Figures 6D, 6E, and S6A). Interestingly, SOX9 or FOXG1 knock down markedly diminished both *BRD4* and c-MYC protein levels in U87EGFRvIII GBM cells (Figures 6F and 6G). Taken together, these results demonstrate that EGFRvIII controls c-MYC levels through SOX9 and FOXG1 mediated regulation of *BRD4*,

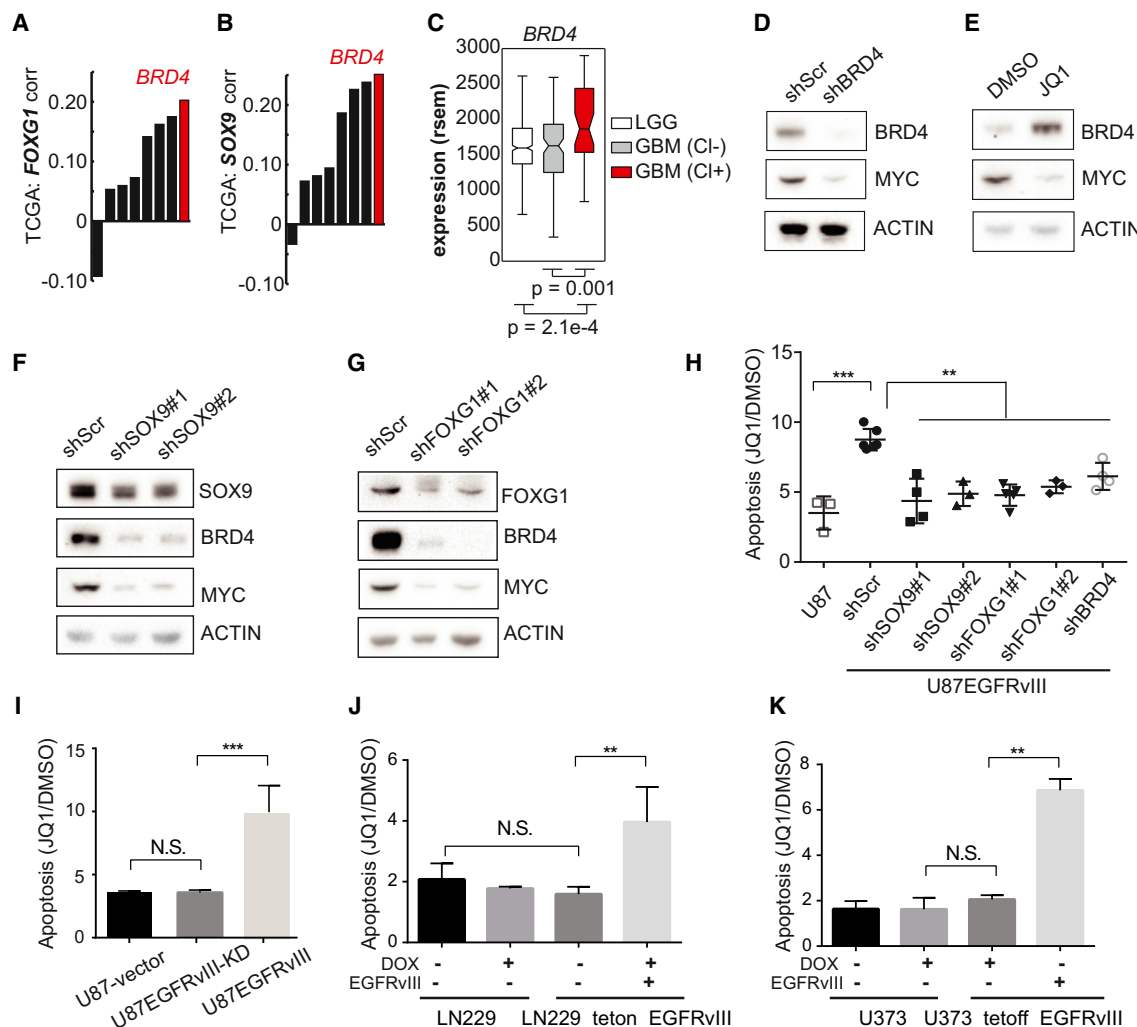


**Figure 6. EGFRvIII Sensitizes GBMs to the BET-Bromodomain Inhibitor JQ1**

(A–C) Correlation of *BRD4* with *SOX9* and *FOGX1* in TCGA GBM gene expression data.

(D and E) Western blots indicate that *BRD4* knockdown decreases c-MYC in U87EGFRvIII cells. The JQ1 treatment (1  $\mu$ M) for 48 hr decreases c-MYC while increasing the level of *BRD4*, suggesting that *BRD4* histone-binding activity is essential for the expression of c-MYC.

(F and G) Western blots show that *BRD4* and c-MYC are depleted by *SOX9* or *FOGX1* knockdown in U87EGFRvIII cells.

(H) Annexin V/PI FACS analysis of apoptotic cells in a series of stable cell lines following 5-day treatment with 1  $\mu$ M JQ1. The U87EGFRvIII cells experienced significantly higher apoptosis levels compared to all the other cell lines (\*\*: p < 0.01, \*\*\*: p < 0.001, and ANOVA test with Dunnett's multiple comparison test). The error bars represent SD.

(I) Heightened sensitivity to JQ1 relies on EGFRvIII's kinase activity (\*\*p < 0.01, \*\*\*p < 0.001, N.S.: not significant, and t test). The error bars represent SD.

(J and K) Inducible EGFRvIII-expressing GBM cell lines are sensitive to JQ1-induced apoptosis (\*\*p < 0.01, not significant: N.S., and t test). The error bars represent SD. See also Figure S6.

consistent with recent evidence that c-MYC is critical for EGFRvIII-dependent tumorigenesis (Babic et al., 2013; Masui et al., 2013).

Recent studies have shown that JQ1 is effective in suppressing the growth of certain cancers that rely on amplified transcription for maintaining their oncogenic state (Lin et al., 2012; Lovén et al., 2013). Therefore, we asked whether EGFRvIII sensitizes GBMs to JQ1 and whether this is mediated through the *SOX9* and *FOGX1* transcriptional network. In U87 GBM cells, the presence of EGFRvIII significantly increased the amount of apoptosis in response to JQ1 (Figures 6H and S6B). shRNAs targeting *SOX9*, *FOGX1*, or *BRD4* all reversed the EGFRvIII-depen-

dent apoptotic sensitivity to JQ1 (Figure 6H), demonstrating that EGFRvIII-expressing GBM cells have heightened apoptotic responsiveness to JQ1, which is mediated by *SOX9* and *FOGX1* and is *BRD4*-dependent. This heightened response to JQ1 is attributable to the kinase activity of EGFRvIII, because no difference was observed in the level of JQ1-induced cell death in U87 GBM cells expressing kinase dead EGFRvIII (Figure 6I). The effect of EGFRvIII on sensitizing GBM cells to JQ1 was also observed in LN229 and U373 GBM cells in which EGFRvIII was under the control of doxycycline-regulatable promoters (LN229 tet-on and U373 tet-off; Figures 6J and 6K).

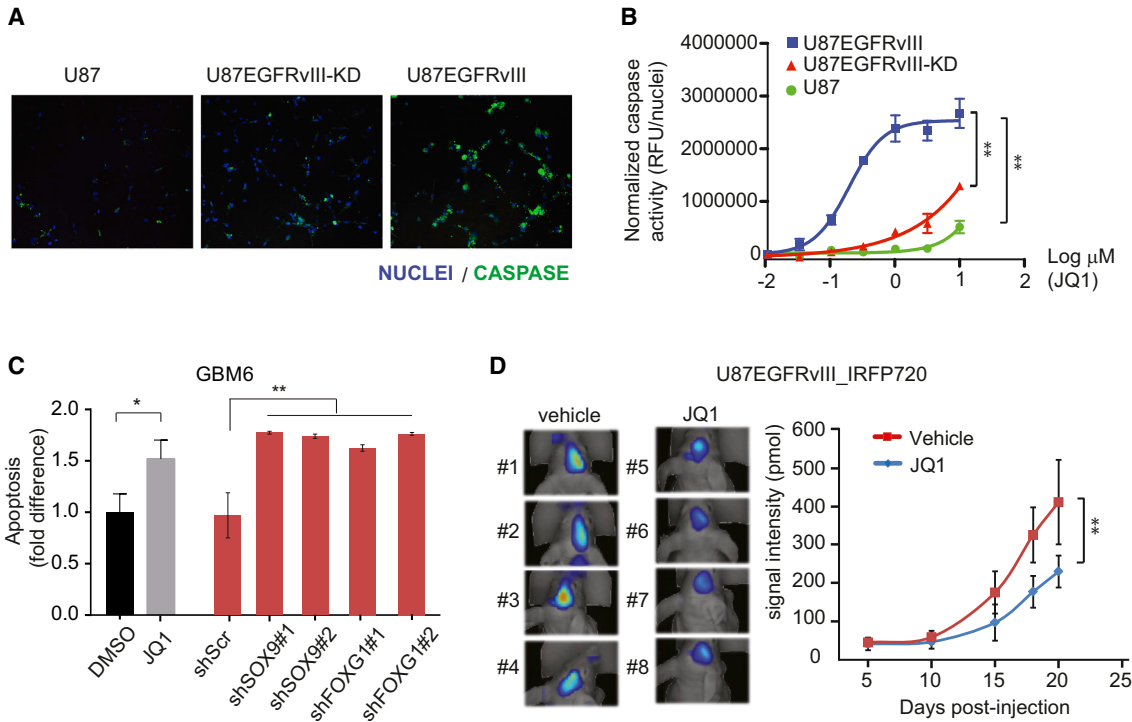


**Figure 7. JQ1 Suppresses EGFRvIII-Dependent Tumor Growth**

(A) Representative images from the live-cell imaging assay for activated caspase-3/7 (green) in U87 cell lines treated with 0.3  $\mu$ M JQ1. The nuclei are stained with Hoechst (blue). At this inhibitor concentration, high levels of caspase activity are only evident in the EGFRvIII-expressing cells.

(B) JQ1 dose response in caspase activity assay. The JQ1 has minor effects on U87 cells and more potently increases caspase activity in U87 cells expressing catalytically active EGFRvIII relative to those expressing the kinase dead receptor [ $EC_{50}$ (U87 EGFRvIII) = 0.20  $\mu$ M;  $EC_{50}$ (U87 EGFRvIII kinase dead)  $\sim$ 10  $\mu$ M;  $EC_{50}$ (U87)  $\gg$  10  $\mu$ M] ( $**p < 0.0001$  and extra sum of squares F test). The error bars represent SD.

(C) GBM6, a patient-derived GBM neurosphere cell line that endogenously expresses EGFRvIII, is sensitive to JQ1-induced apoptosis. The knock downs of SOX9 or FOXG1 decrease the viability of GBM6 in vitro ( $*p < 0.05$ ,  $**p < 0.01$ , and t test). The error bars represent SD.

(D) FMT fluorescence scan of intracranially transplanted U87EGFRvIII\_irFP720 cells in mice treated with JQ1 or vehicle at 18<sup>th</sup> day post-injection and quantitation of fluorescence intensity of tumors formed by U87EGFRvIII\_irFP720 cells in mice. The vehicle or JQ1 (50 mg/kg of body weight, twice per day) treatment started at the sixth day post-injection (n = 12 per group) ( $**p < 0.01$  and t test). The error bars represent SD. See also Figure S7.

To further confirm these findings, we applied a live-cell activated caspase-3/7 imaging assay to assess whether this JQ1-mediated apoptosis was correlated with increased caspase activation and/or EGFRvIII kinase activity. By this method, JQ1 had only minor effects on U87 cells. In contrast, JQ1 treatment caused dose-dependent increases in caspase activity levels in both U87 EGFRvIII and kinase dead EGFRvIII cells. However, JQ1 exerted its effects on the U87 EGFRvIII cells at significantly lower concentrations relative to those expressing the catalytically inactive mutant (Figures 7A, 7B, and S6C). Hence, the effects of JQ1 on cell death are likely caspase-dependent and dramatically enhanced by EGFRvIII kinase activity. Furthermore, the patient-derived neurosphere cell line GBM6, which carries endogenous EGFR amplification and EGFRvIII mutation, is sensitive to JQ1-induced cell death and its viability is dependent on the expression of SOX9 and FOXG1 (Figure 7C).

Last, we examined the effect of JQ1, which was highly brain-penetrant (Figure S7), on U87 EGFRvIII GBM growth in the brain in a mouse xenograft model. JQ1 administered twice daily at 50 mg/kg by oral gavage significantly decreased intracranial tumor growth (Figure 7D).

## DISCUSSION

Cancer arises from the intertwined processes of spontaneous somatic mutation and sequential selection for aggressive subclones (Stratton, 2011). Cancer is also an epigenetic disease. Mutations in TFs, chromatin regulators, and even non-coding intergenic sequences, including putative super-enhancer sequences, contribute to tumor formation and progression (Lee and Young, 2013; Mansour et al., 2014), consistent with the critical role for epigenetic alterations in tumorigenesis. There is also a complex interplay between genetic and epigenetic mechanisms in cancer, as oncogenes remodel cis-regulatory and TF networks to promote tumor formation and progression (Baylin and Jones, 2011; Hanahan and Weinberg, 2011; Lee and Young, 2013; Rivera and Ren, 2013; Shen and Laird, 2013; Suvà et al., 2013). Currently, the mechanisms by which oncogenic mutations remodel the epigenome are incompletely understood.

Here, we set out to determine the impact of EGFR mutations, one of the signature molecular lesions in GBM, on epigenetic reprogramming. GBM is a particularly compelling tumor for this type of integrated analysis. GBM is one of the most deeply

genomically characterized forms of cancer (Lawrence et al., 2014), revealing a remarkably high prevalence of EGFR amplification and mutations (Brennan et al., 2013), even at the single cell level (Patel et al., 2014). Extensive research has begun to identify the signaling pathways and metabolic events by which EGFR mutations promote GBM pathogenesis (Cloughesy et al., 2014; Furnari et al., 2015). However, the global impact of EGFR mutations on epigenetic remodeling in GBM is not understood. Therefore, we applied global RNA-seq and ChIP-seq approaches to GBM cell lines, patient-derived tumor cells in neurosphere culture, and clinical biopsies genotyped for EGFR mutation status to interrogate the global impact of EGFRvIII on epigenetic remodeling, revealing a SOX9 and FOXG1-dependent transcriptional regulatory network that remodels the enhancer activation landscape to drive EGFRvIII-dependent tumorigenesis.

There are likely to be many other epigenetic states and TFs that are critical for GBM pathogenesis, including the ones recently described that control the stem-like state and in vivo tumor propagation capacity (Rheinbay et al., 2013; Suvà et al., 2014). We have previously shown that endogenously expressed EGFRvIII does not appear to alter the stem-like state of GBM cells (Nathanson et al., 2014). Thus, it is not surprising that our analyses might not pick up those previously detected critical TF networks involved in stem cell fate reprogramming. Instead, our study enabled us to detect a critical transcription network and epigenetic state by which EGFRvIII promotes tumor formation and progression.

EGFR mutations, including EGFRvIII, are compelling drug targets in GBM. However, EGFR tyrosine kinase inhibitors have failed to show durable benefit for GBM patients in part because it has not been possible to achieve sufficient intratumoral drug levels to adequately inhibit EGFR phosphorylation (Vivanco et al., 2012). This failure of target inhibition results in feedback activation of other RTKs such as PDGFR $\beta$  to maintain downstream signal flux and/or reversible loss of EGFRvIII from extra-chromosomal DNA to promote drug resistance (Akhavan et al., 2013; Furnari et al., 2015; Nathanson et al., 2014). Until new drug formulations or better dosing approaches are developed that safely achieve higher dose levels and more effectively target inhibition within the tumor in the brain, alternative therapeutic strategies for EGFR activated GBMs need to be considered.

Our finding that EGFRvIII sensitizes GBM cells to the BET-bromodomain inhibitor, suggests a potentially clinically actionable “precision medicine” strategy. We find that EGFRvIII enhances JQ1-dependent apoptosis via its effect on SOX9 and FOXG1, which converge to control BRD4 and c-MYC protein levels. JQ1 treatment results in a near total loss of c-MYC protein on western blot (Figure 6D), whereas the decrement in c-MYC transcript is more modest (Figure S6A). Similarly, SOX9 and FOXG1 knock downs precipitously lower c-MYC protein levels (Figures 6F and 6G), despite relatively modest effects on expression of c-MYC transcript. These observations, although limited in scope, raise the possibility that SOX9 and FOXG1 may regulate c-MYC protein translation and/or stability in a BRD4- (or other BET bromodomain protein) dependent fashion. Future studies will be needed to test this possibility, to determine if it is detected in other cell contexts, and to identify a potential underlying mechanism.

Many cancer types depend on c-MYC for growth and proliferation, and c-MYC is a common target for amplification in many

of these tumors (Lee and Young, 2013; Lin et al., 2012; Nie et al., 2012). In contrast in GBM, c-MYC is rarely amplified or mutated (Brennan et al., 2013). We have previously demonstrated that EGFRvIII signaling through mTORC1 enhances c-MYC activity through the alternative splicing of the c-MYC heterodimerization partner Max to generate Delta Max, a gain of function variant (Babic et al., 2013). Further, EGFRvIII controls c-MYC protein level through a FOXO 1-, 3-acetylation signaling cascade (Masui et al., 2013). Thus, our finding that EGFRvIII regulates c-MYC levels through the SOX9 and FOXG1 transcriptional activity further demonstrates the critical nature of c-MYC in EGFRvIII-dependent GBM pathogenesis, expands our understanding of its regulation, and potentially explains the enhanced apoptotic sensitivity to JQ1. It is also interesting to speculate that BRD4 and elevated c-MYC activity downstream of growth factor receptor mutations in adult GBMs may be a common pathogenic mechanism shared with pediatric high grade gliomas that have H3K27M mutations, but lack growth factor receptor alterations (Herz et al., 2014; Lewis et al., 2013; Sturm et al., 2014).

## EXPERIMENTAL PROCEDURES

### Cell Lines and Tissue Samples

The human glioma cell line U87 (or U-87MG) was purchased from ATCC. U87EGFRvIII, U87EGFRvIII-KD, LN229\_teton\_vIII, U373\_tetoff\_vIII, and GBM6 cell lines were described before (Akhavan et al., 2013; Nathanson et al., 2014; Wang et al., 2006). Tumor samples were obtained from University of California, Los Angeles (UCLA) Brain Tumor Translational Resource. Normal brain tissues were obtained from the National Institute of Child Health and Human Development (NICHD) Brain Bank for Developmental Disorders. Ethics approval was obtained from the UCLA for use of the GBM tumor samples and from the University Health Network and the Hospital for Sick Children for use of the normal brain tissues.

### RNA-Seq

Total RNA was extracted from one–two million cells cultured in petri dish or 50–100 mg of tissue using the RNeasy mini kit (QIAGEN). There were 5~10  $\mu$ g of total RNA that were used to prepare RNA-seq libraries according to Illumina protocol. There were 4–6 libraries that were mixed for multiplexed pair-end sequencing using Illumina HiSeq 2000 (Illumina).

### ChIP-Seq and ChIP-qPCR

ChIP was performed as previously described (Heintzman et al., 2007). Immunoprecipitated DNA was purified after phenol extraction and was used for qPCR (KAPA Biosystems) or for preparing barcoded high throughput sequencing libraries according to Illumina protocols with minor modifications. There were 4–12 library preps that were mixed for multiplexed single-read sequencing using Illumina Hi-seq 2000 (Illumina). Antibodies used for ChIP were polyclonal rabbit anti-H3K27ac (Active Motif, Cat#39133), polyclonal rabbit anti-H3K4me3 (Active Motif, Cat#39159), polyclonal rabbit anti-H3K4me1 (Abcam, Cat#8895), monoclonal rabbit IgG (Abcam, Cat#ab172730), polyclonal rabbit anti-SOX9 (Millipore, Cat#AB5535), and polyclonal rabbit anti-FOGX1 (Pierce, Cat# PA5-26794).

### ChIP-Seq Analysis

For a given locus, histone modification enrichment is quantified as  $E = \log_2(\text{ChIP RPKM} / \text{input RPKM})$ , where RPKM is defined as the number of reads per kilobase of locus per million mapped reads, in either ChIP or input samples. To avoid division by zero, a pseudocount of 0.05 is added to both numerator and denominator. Given a set of differentially expressed genes, we created a set of bins  $\pm 500$  kb from the transcription start sites of these genes. We also repeated this process to create 5,000 random sets of bins corresponding to the same number of random genes. Given a set of enhancers, we assessed enrichment by overlapping with

bins of differentially expressed genes and comparing with the overlap for random bin sets. Motif finding was performed using Homer v4.2 (Heinz et al., 2010).

### RNA-Seq Analysis

For pairwise comparisons between two sets of samples, the number of sense exonic reads were quantified and input to edgeR (Robinson et al., 2010) to normalize and call differentially expressed genes at a p value cutoff of 0.05. To perform GSEA of RNA-seq data on U87EGFRvIII<sup>shSOX9</sup> or U87EGFRvIII<sup>shFOXG1</sup> compared to U87EGFRvIII, we represented expression of genes as the mean of RPKM values from biological replicates, calculated the log ratio of knockdown to U87EGFRvIII cells, and ran GSEA v2.1.0 (Subramanian et al., 2005).

### TCGA Data Analysis

Processed TCGA data were downloaded through the TCGA data portal, and mapped RNA-seq BAM files were acquired through the Cancer Genomics Hub (<https://cghub.ucsc.edu/>). The EGFR status of TCGA samples are designated as euploid, regionally amplified, focally amplified, or EGFRvIII based on annotations previously published (Brennan et al., 2013). Specifically, EGFRvIII samples are samples with non-zero Δ2–7 values, and euploid / regionally amplified / focally amplified samples are non-EGFRvIII samples labeled as “Euploid” / “Regional gain” / “Focal Amplification.” Random forest analysis was performed using the TreeBagger function defined in Matlab. Given the expression of RTKs known to be amplified in a given cancer type as described in the TCGA Copy Number Portal (Mermel et al., 2011), the random forest was first trained and then used to predict whether each sample is a high (top 100) or low (bottom 100) expresser of SOX9/FOXG1.

### Intracranial Xenograft

Athymic nu/nu mice 5 weeks of age were purchased from Harlan Sprague Dawley Inc. There were  $1 \times 10^5$  U87EGFRvIII\_iRFP720 cells in 5 μl of phosphate-buffered saline (PBS) that were intracranially injected to the mouse brain (Ozawa and James, 2010). Tumor growth was monitored using an FMT 2500 Fluorescence Tomography System (PerkinElmer). For drug treatment studies, vehicle (10% of hydroxypropyl beta cyclodextrin, Sigma-Aldrich Cat#: C0926-10G) or JQ1 (5 mg/ml) were administered to mice (10 μl per gram of body weight, or 50 mg/kg) via gavage twice daily starting from the sixth day post-injection. All procedures have been reviewed and approved by the Institutional Animal Use and Care Committee at University of California San Diego.

### ACCESSION NUMBERS

The ChIP-seq and RNA-seq data reported in this study have been deposited with the Gene Expression Omnibus under the accession GEO ID: GSE72468.

### SUPPLEMENTAL INFORMATION

Supplemental Information includes Supplemental Experimental Procedures, seven figures, and four tables and can be found with this article online at <http://dx.doi.org/10.1016/j.molcel.2015.09.002>.

### AUTHOR CONTRIBUTIONS

F.L., G.C.H., B.R., and P.S.M. conceived the project and designed the research. F.L., G.R.V., K.M.T., S.I., H.Y., Z.Y., A.Y.L., C.Z., and D.J. performed experiments. G.C.H. and B.L. conducted high-throughput sequencing data analysis. C.L.B., B.W., G.L., T.F.C., and W.H.Y. provided tissue samples, clinical information, and helped with interpretation of data. F.B.F., T.C.G., W.Z., A.K.S., and W.K.C. provided new reagents and analytic tools and provided intellectual contributions to design of experiments and interpretation of data. F.L., G.C.H., A.K.S., W.K.C., B.R., and P.S.M. wrote the paper. All authors discussed the results and commented on the manuscript.

### ACKNOWLEDGMENTS

The infrared Fluorescent Protein 720 (IRFP720) expression construct was kindly given by Dr. V.V. Verkusha. This work is supported by the National Institute for

Neurological Diseases and Stroke grant NS73831 (to P.S.M.); the Defeat GBM Program of the National Brain Tumor Society and generous donations from the Ziering Family Foundation in memory of Sigi Ziering (to P.S.M. and T.F.C.); the Ben and Catherine Ivy Foundation (to P.S.M., T.F.C., and W.H.Y.); the Ludwig Institute for Cancer Research (to B.R., A.K.S., and T.C.G.); the Cancer Prevention and Research Institute of Texas grant RR140023 (to G.C.H.); UCSD Core Facility Stimulus Funding (to B.R.); the NIH grant R01-NS080939 (to F.B.F.); the National Cancer Institute grant F31CA186668 (to G.R.V.); the Hospital for Sick Children Psychiatric Endowment Fund (to C.L.B.); Art of the Brain (to T.F.C. and W.H.Y.); and the Uncle Kory Foundation (to T.F.C.). W.K.C. is a Fellow of the National Foundation for Cancer Research.

Received: January 16, 2015

Revised: June 2, 2015

Accepted: September 1, 2015

Published: October 8, 2015

### REFERENCES

- Akhavan, D., Pourzia, A.L., Nourian, A.A., Williams, K.J., Nathanson, D., Babic, I., Villa, G.R., Tanaka, K., Nael, A., Yang, H., et al. (2013). De-repression of PDGFR $\beta$  transcription promotes acquired resistance to EGFR tyrosine kinase inhibitors in glioblastoma patients. *Cancer Discov.* 3, 534–547.
- Babic, I., Anderson, E.S., Tanaka, K., Guo, D., Masui, K., Li, B., Zhu, S., Gu, Y., Villa, G.R., Akhavan, D., et al. (2013). EGFR mutation-induced alternative splicing of Max contributes to growth of glycolytic tumors in brain cancer. *Cell Metab.* 17, 1000–1008.
- Baylin, S.B., and Jones, P.A. (2011). A decade of exploring the cancer epigenome - biological and translational implications. *Nat. Rev. Cancer* 11, 726–734.
- Brennan, C.W., Verhaak, R.G., McKenna, A., Campos, B., Noushmehr, H., Salama, S.R., Zheng, S., Chakravarty, D., Sanborn, J.Z., Berman, S.H., et al.; TCGA Research Network (2013). The somatic genomic landscape of glioblastoma. *Cell* 155, 462–477.
- Ciriello, G., Miller, M.L., Aksoy, B.A., Senbabaooglu, Y., Schultz, N., and Sander, C. (2013). Emerging landscape of oncogenic signatures across human cancers. *Nat. Genet.* 45, 1127–1133.
- Cloughesy, T.F., Cavenee, W.K., and Mischel, P.S. (2014). Glioblastoma: from molecular pathology to targeted treatment. *Annu. Rev. Pathol.* 9, 1–25.
- Creyghton, M.P., Cheng, A.W., Welstead, G.G., Kooistra, T., Carey, B.W., Steine, E.J., Hanna, J., Lodato, M.A., Frampton, G.M., Sharp, P.A., et al. (2010). Histone H3K27ac separates active from poised enhancers and predicts developmental state. *Proc. Natl. Acad. Sci. USA* 107, 21931–21936.
- Delmore, J.E., Issa, G.C., Lemieux, M.E., Rahl, P.B., Shi, J., Jacobs, H.M., Kastritis, E., Gilpatrick, T., Paran, R.M., Qi, J., et al. (2011). BET bromodomain inhibition as a therapeutic strategy to target c-Myc. *Cell* 146, 904–917.
- Filippakopoulos, P., Qi, J., Picaud, S., Shen, Y., Smith, W.B., Fedorov, O., Morse, E.M., Keates, T., Hickman, T.T., Felletar, I., et al. (2010). Selective inhibition of BET bromodomains. *Nature* 468, 1067–1073.
- Furnari, F.B., Cloughesy, T.F., Cavenee, W.K., and Mischel, P.S. (2015). Heterogeneity of epidermal growth factor receptor signalling networks in glioblastoma. *Nat. Rev. Cancer* 15, 302–310.
- Guo, W., Keckesova, Z., Donaher, J.L., Shibue, T., Tischler, V., Reinhardt, F., Itzkovitz, S., Noske, A., Zürner-Härdi, U., Bell, G., et al. (2012). Slug and Sox9 cooperatively determine the mammary stem cell state. *Cell* 148, 1015–1028.
- Hanahan, D., and Weinberg, R.A. (2011). Hallmarks of cancer: the next generation. *Cell* 144, 646–674.
- Heintzman, N.D., Stuart, R.K., Hon, G., Fu, Y., Ching, C.W., Hawkins, R.D., Barrera, L.O., Van Calcar, S., Qu, C., Ching, K.A., et al. (2007). Distinct and predictive chromatin signatures of transcriptional promoters and enhancers in the human genome. *Nat. Genet.* 39, 311–318.
- Heinz, S., Benner, C., Spann, N., Bertolino, E., Lin, Y.C., Laslo, P., Cheng, J.X., Murre, C., Singh, H., and Glass, C.K. (2010). Simple combinations of lineage-determining transcription factors prime cis-regulatory elements required for macrophage and B cell identities. *Mol. Cell* 38, 576–589.

- Herz, H.M., Morgan, M., Gao, X., Jackson, J., Rickels, R., Swanson, S.K., Florens, L., Washburn, M.P., Eissenberg, J.C., and Shilatifard, A. (2014). Histone H3 lysine-to-methionine mutants as a paradigm to study chromatin signaling. *Science* 345, 1065–1070.
- Huang, H.S., Nagane, M., Klingbeil, C.K., Lin, H., Nishikawa, R., Ji, X.D., Huang, C.M., Gill, G.N., Wiley, H.S., and Cavenee, W.K. (1997). The enhanced tumorigenic activity of a mutant epidermal growth factor receptor common in human cancers is mediated by threshold levels of constitutive tyrosine phosphorylation and unattenuated signaling. *J. Biol. Chem.* 272, 2927–2935.
- Kandoth, C., McLellan, M.D., Vandin, F., Ye, K., Niu, B., Lu, C., Xie, M., Zhang, Q., McMichael, J.F., Wyczalkowski, M.A., et al. (2013). Mutational landscape and significance across 12 major cancer types. *Nature* 502, 333–339.
- Lawrence, M.S., Stojanov, P., Mermel, C.H., Robinson, J.T., Garraway, L.A., Golub, T.R., Meyerson, M., Gabriel, S.B., Lander, E.S., and Getz, G. (2014). Discovery and saturation analysis of cancer genes across 21 tumor types. *Nature* 505, 495–501.
- Lee, T.I., and Young, R.A. (2013). Transcriptional regulation and its misregulation in disease. *Cell* 152, 1237–1251.
- Lewis, P.W., Müller, M.M., Koletsky, M.S., Cordero, F., Lin, S., Banaszynski, L.A., Garcia, B.A., Muir, T.W., Becher, O.J., and Allis, C.D. (2013). Inhibition of PRC2 activity by a gain-of-function H3 mutation found in pediatric glioblastoma. *Science* 340, 857–861.
- Lin, C.Y., Lovén, J., Rahl, P.B., Paraná, R.M., Burge, C.B., Bradner, J.E., Lee, T.I., and Young, R.A. (2012). Transcriptional amplification in tumor cells with elevated c-Myc. *Cell* 151, 56–67.
- Lovén, J., Hoke, H.A., Lin, C.Y., Lau, A., Orlando, D.A., Vakoc, C.R., Bradner, J.E., Lee, T.I., and Young, R.A. (2013). Selective inhibition of tumor oncogenes by disruption of super-enhancers. *Cell* 153, 320–334.
- Mansour, M.R., Abraham, B.J., Anders, L., Berezovskaya, A., Gutierrez, A., Durbin, A.D., Etchin, J., Lawton, L., Sallan, S.E., Silverman, L.B., et al. (2014). Oncogene regulation. An oncogenic super-enhancer formed through somatic mutation of a noncoding intergenic element. *Science* 346, 1373–1377.
- Masui, K., Tanaka, K., Akhavan, D., Babic, I., Gini, B., Matsutani, T., Iwanami, A., Liu, F., Villa, G.R., Gu, Y., et al. (2013). mTOR complex 2 controls glycolytic metabolism in glioblastoma through FoxO acetylation and upregulation of c-Myc. *Cell Metab.* 18, 726–739.
- Mermel, C.H., Schumacher, S.E., Hill, B., Meyerson, M.L., Beroukhim, R., and Getz, G. (2011). GISTIC2.0 facilitates sensitive and confident localization of the targets of focal somatic copy-number alteration in human cancers. *Genome Biol.* 12, R41.
- Nathanson, D.A., Gini, B., Mottahedeh, J., Visnyei, K., Koga, T., Gomez, G., Eskin, A., Hwang, K., Wang, J., Masui, K., et al. (2014). Targeted therapy resistance mediated by dynamic regulation of extrachromosomal mutant EGFR DNA. *Science* 343, 72–76.
- Nie, Z., Hu, G., Wei, G., Cui, K., Yamane, A., Resch, W., Wang, R., Green, D.R., Tessarollo, L., Casellas, R., et al. (2012). c-Myc is a universal amplifier of expressed genes in lymphocytes and embryonic stem cells. *Cell* 151, 68–79.
- Ozawa, T., and James, C.D. (2010). Establishing intracranial brain tumor xenografts with subsequent analysis of tumor growth and response to therapy using bioluminescence imaging. *J. Vis. Exp.* (41), 1986.
- Parker, B.C., Annala, M.J., Cogdell, D.E., Granberg, K.J., Sun, Y., Ji, P., Li, X., Gumin, J., Zheng, H., Hu, L., et al. (2013). The tumorigenic FGFR3-TACC3 gene fusion escapes miR-99a regulation in glioblastoma. *J. Clin. Invest.* 123, 855–865.
- Patel, A.P., Tirosh, I., Trombetta, J.J., Shalek, A.K., Gillespie, S.M., Wakimoto, H., Cahill, D.P., Nahed, B.V., Curry, W.T., Martuza, R.L., et al. (2014). Single-cell RNA-seq highlights intratumoral heterogeneity in primary glioblastoma. *Science* 344, 1396–1401.
- Rada-Iglesias, A., Bajpai, R., Swigut, T., Brugmann, S.A., Flynn, R.A., and Wysocka, J. (2011). A unique chromatin signature uncovers early developmental enhancers in humans. *Nature* 470, 279–283.
- Rani, S.B., Rathod, S.S., Karthik, S., Kaur, N., Muzumdar, D., and Shiras, A.S. (2013). MiR-145 functions as a tumor-suppressive RNA by targeting Sox9 and adducin 3 in human glioma cells. *Neuro-oncol.* 15, 1302–1316.
- Rheinbay, E., Suvà, M.L., Gillespie, S.M., Wakimoto, H., Patel, A.P., Shahid, M., Oksuz, O., Rabkin, S.D., Martuza, R.L., Rivera, M.N., et al. (2013). An aberrant transcription factor network essential for Wnt signaling and stem cell maintenance in glioblastoma. *Cell Rep.* 3, 1567–1579.
- Rivera, C.M., and Ren, B. (2013). Mapping human epigenomes. *Cell* 155, 39–55.
- Robinson, M.D., McCarthy, D.J., and Smyth, G.K. (2010). edgeR: a Bioconductor package for differential expression analysis of digital gene expression data. *Bioinformatics* 26, 139–140.
- Sarkaria, J.N., Yang, L., Grogan, P.T., Kitange, G.J., Carlson, B.L., Schroeder, M.A., Galanis, E., Giannini, C., Wu, W., Dinca, E.B., and James, C.D. (2007). Identification of molecular characteristics correlated with glioblastoma sensitivity to EGFR kinase inhibition through use of an intracranial xenograft test panel. *Mol. Cancer Ther.* 6, 1167–1174.
- Seoane, J., Le, H.V., Shen, L., Anderson, S.A., and Massagué, J. (2004). Integration of Smad and forkhead pathways in the control of neuroepithelial and glioblastoma cell proliferation. *Cell* 117, 211–223.
- Shen, H., and Laird, P.W. (2013). Interplay between the cancer genome and epigenome. *Cell* 153, 38–55.
- Shi, J., and Vakoc, C.R. (2014). The mechanisms behind the therapeutic activity of BET bromodomain inhibition. *Mol. Cell* 54, 728–736.
- Singh, D., Chan, J.M., Zoppoli, P., Niola, F., Sullivan, R., Castano, A., Liu, E.M., Reichel, J., Porriati, P., Pellegatta, S., et al. (2012). Transforming fusions of FGFR and TACC genes in human glioblastoma. *Science* 337, 1231–1235.
- Stratton, M.R. (2011). Exploring the genomes of cancer cells: progress and promise. *Science* 331, 1553–1558.
- Sturm, D., Bender, S., Jones, D.T., Lichter, P., Grill, J., Becher, O., Hawkins, C., Majewski, J., Jones, C., Costello, J.F., et al. (2014). Paediatric and adult glioblastoma: multifiform (epi)genomic culprits emerge. *Nat. Rev. Cancer* 14, 92–107.
- Subramanian, A., Tamayo, P., Mootha, V.K., Mukherjee, S., Ebert, B.L., Gillette, M.A., Paulovich, A., Pomeroy, S.L., Golub, T.R., Lander, E.S., and Mesirov, J.P. (2005). Gene set enrichment analysis: a knowledge-based approach for interpreting genome-wide expression profiles. *Proc. Natl. Acad. Sci. USA* 102, 15545–15550.
- Suvà, M.L., Riggi, N., and Bernstein, B.E. (2013). Epigenetic reprogramming in cancer. *Science* 339, 1567–1570.
- Suvà, M.L., Rheinbay, E., Gillespie, S.M., Patel, A.P., Wakimoto, H., Rabkin, S.D., Riggi, N., Chi, A.S., Cahill, D.P., Nahed, B.V., et al. (2014). Reconstructing and reprogramming the tumor-propagating potential of glioblastoma stem-like cells. *Cell* 157, 580–594.
- Swartling, F.J., Savov, V., Persson, A.I., Chen, J., Hackett, C.S., Northcott, P.A., Grimmer, M.R., Lau, J., Chesler, L., Perry, A., et al. (2012). Distinct neural stem cell populations give rise to disparate brain tumors in response to N-MYC. *Cancer Cell* 21, 601–613.
- Verdinelli, F., Perin, A., Dali, R., Fung, K.H., Lo, R., Longatti, P., Guiot, M.C., Del Maestro, R.F., Rossi, S., di Porzio, U., et al. (2013). Transcription factors FOXG1 and Groucho/TLE promote glioblastoma growth. *Nat. Commun.* 4, 2956.
- Vivanco, I., Robins, H.I., Rohle, D., Campos, C., Grommes, C., Nghiemphu, P.L., Kubek, S., Oldrini, B., Chheda, M.G., Yannuzzi, N., et al. (2012). Differential sensitivity of glioma- versus lung cancer-specific EGFR mutations to EGFR kinase inhibitors. *Cancer Discov.* 2, 458–471.
- Vogelstein, B., Papadopoulos, N., Velculescu, V.E., Zhou, S., Diaz, L.A., Jr., and Kinzler, K.W. (2013). Cancer genome landscapes. *Science* 339, 1546–1558.
- Wang, M.Y., Lu, K.V., Zhu, S., Dia, E.Q., Vivanco, I., Shackleford, G.M., Cavenee, W.K., Mellingtonhoff, I.K., Cloughesy, T.F., Sawyers, C.L., and Mischel, P.S. (2006). Mammalian target of rapamycin inhibition promotes response to epidermal growth factor receptor kinase inhibitors in PTEN-deficient and PTEN-intact glioblastoma cells. *Cancer Res.* 66, 7864–7869.
- Wang, L., He, S., Yuan, J., Mao, X., Cao, Y., Zong, J., Tu, Y., and Zhang, Y. (2012). Oncogenic role of SOX9 expression in human malignant glioma. *Med. Oncol.* 29, 3484–3490.

**Supplemental Information**

**EGFR Mutation Promotes Glioblastoma through Epigenome and Transcription Factor Network**

**Remodeling**

Feng Liu, Gary C. Hon, Genaro R. Villa, Kristen M. Turner, Shiro Ikegami, Huijun Yang, Zhen Ye, Bin Li, Samantha Kuan, Ah Young Lee, Ciro Zanca, Bowen Wei, Greg Lucey, David Jenkins, Wei Zhang, Cathy L. Barr, Frank B. Furnari, Timothy F. Cloughesy, William H. Yong, Timothy C. Gahman, Andrew K. Shiau, Webster K. Cavenee, Bing Ren, and Paul S. Mischel

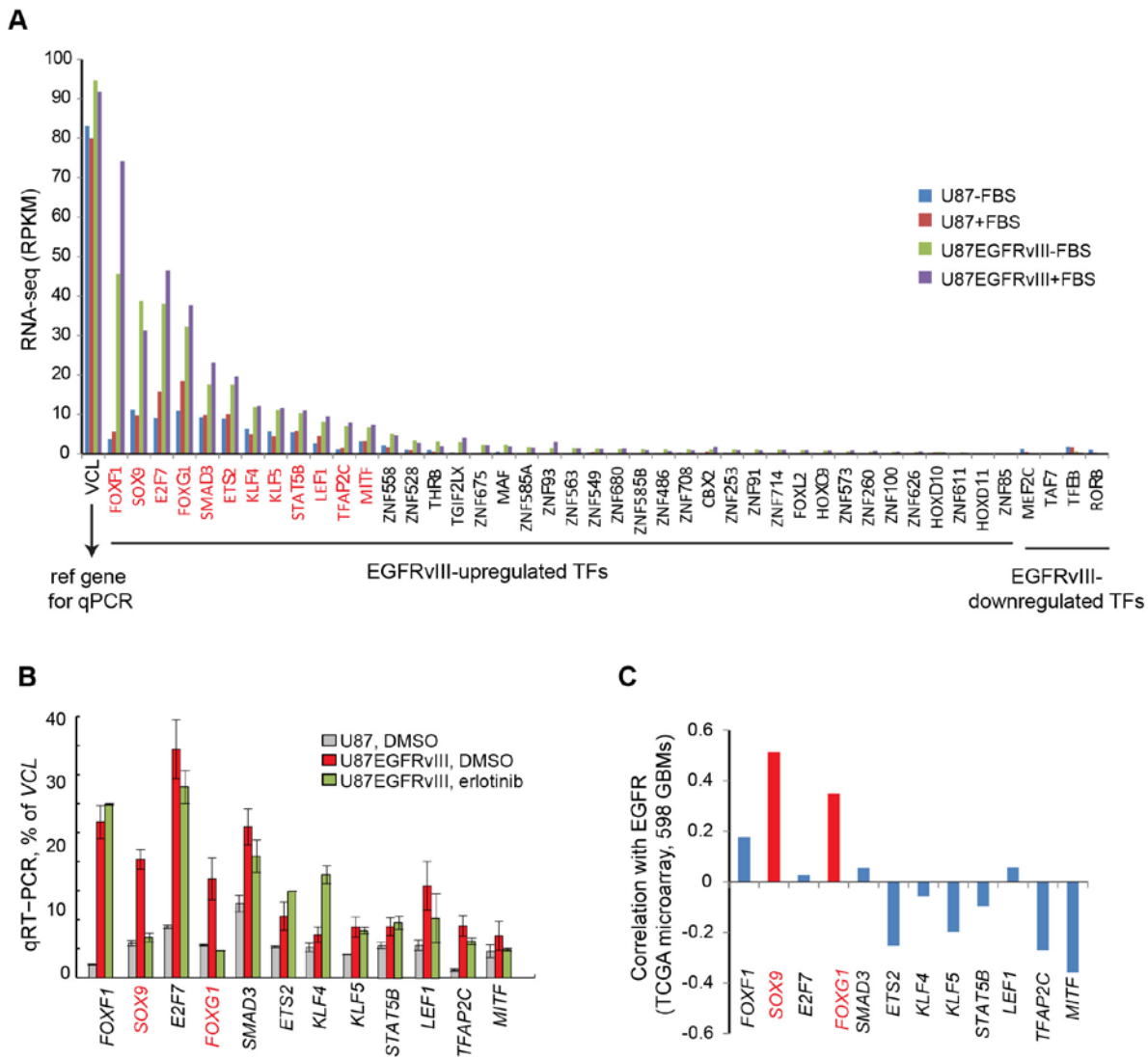


**Figure S1, related to Figure 1.** EGFRvIII-regulated transcription factors (TFs). **(A)** RNA-seq data of genes encoding DNA-sequence specific binding TFs. The y-axis shows reads per kilo bases per million reads (RPKM). EGFRvIII up- and down-regulated TFs are indicated below. *VINCULIN* (*VCL*) does not show significant differences between U87 and U87EGFRvIII cells, and is included as negative control. **(B)** Response of 12 EGFRvIII-activated TFs to 24 hr of 10 uM erlotinib treatment. Only the levels of *SOX9* and *FOXG1* decreased to the base levels in U87. **(C)** *SOX9* and *FOXG1* transcript levels are also most positively correlated with *EGFR* in 598 GBM tumors in the TCGA database.

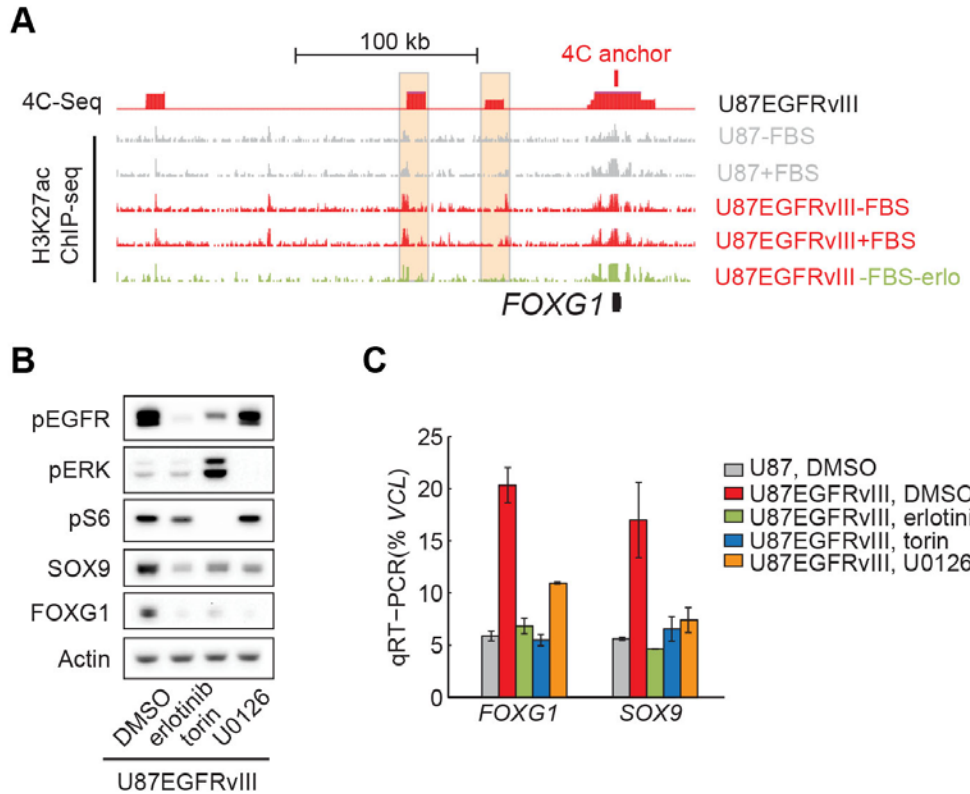


**Figure S2, related to Figure 2.** **(A)** Two EGFRvIII-responsive enhancers near the *FOXG1* locus interact with the promoter of *FOXG1*, as shown by the circularized chromosome confirmation capture assay followed by high-throughput sequencing (4C-Seq). **(B)** Western blots of cells treated by EGFR pathway inhibitors for 24 hours. Erlotinib (10  $\mu$ M) is a tyrosine kinase inhibitor of EGFR/EGFRvIII. Torin (0.25  $\mu$ M) is an mTOR (mTOR1/2) inhibitor. U0126 (10  $\mu$ M) is a MEK inhibitor. pEGFR, pERK, and pS6 were used to monitor the effectiveness of the compounds at the doses used in the experiments. **(C)** qRT-PCR experiments indicate that these kinase inhibitors suppress SOX9 and FOXG1 at the level of transcription.

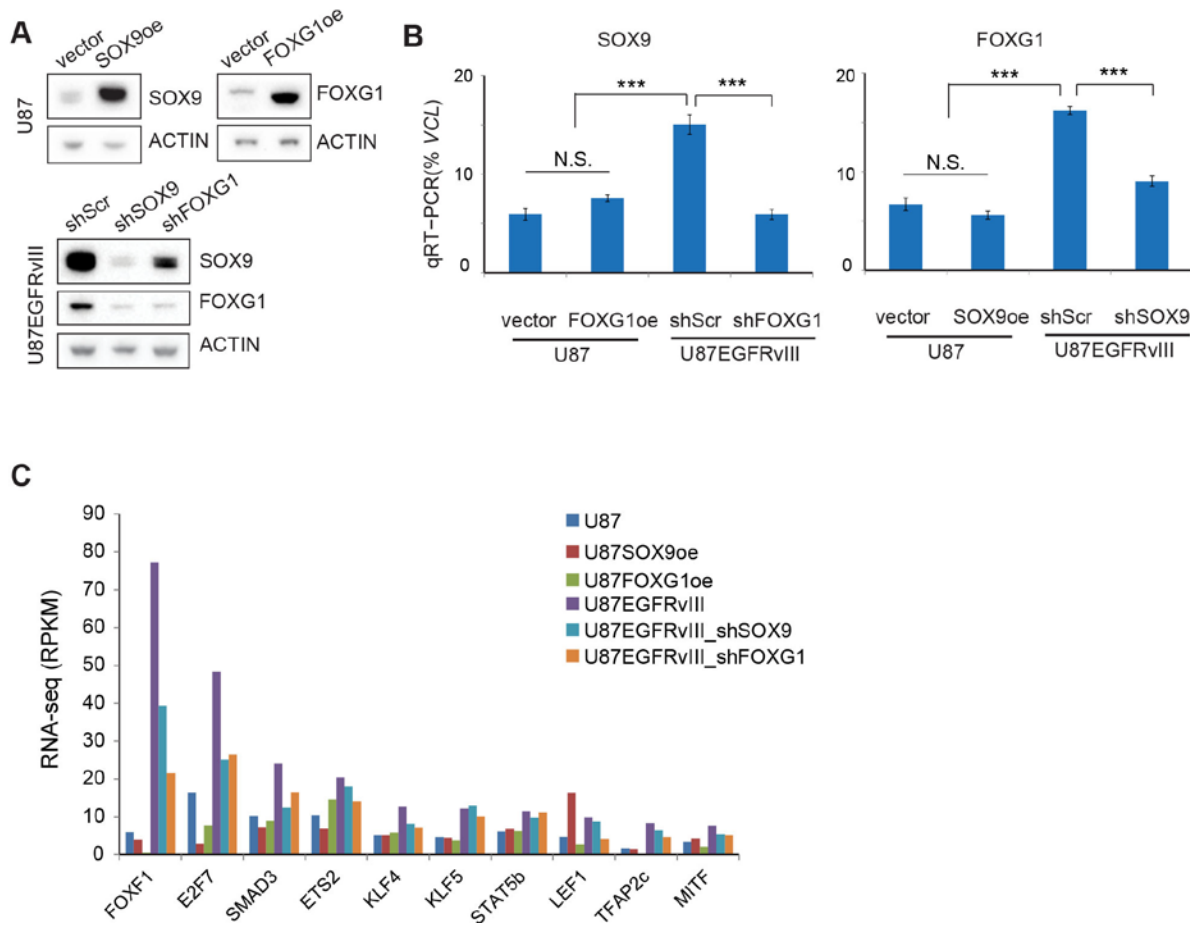


**Figure S3, related to Figure 3.** **(A)** Western blots of U87 cells over-expressing SOX9 or FOXG1, or U87EGFRvIII cells expression short hairpins targeting SOX9 and FOXG1. **(B)** qRT-PCR experiments indicate that overexpression of SOX9 or FOXG1 is insufficient to activate each other in U87 cells. However, in U87EGFRvIII cells, SOX9 is required for the expression of FOXG1, and vice versa. \*\*\*:  $p<0.001$ ,  $t$ -test. N.S.: not significant. **(C)** RNA-seq data of the top 12 EGFRvIII-activated TFs in U87 cells overexpressing SOX9 or FOXG1, as well as in U87EGFRvIII cells with SOX9 and FOXG1 knockdown.

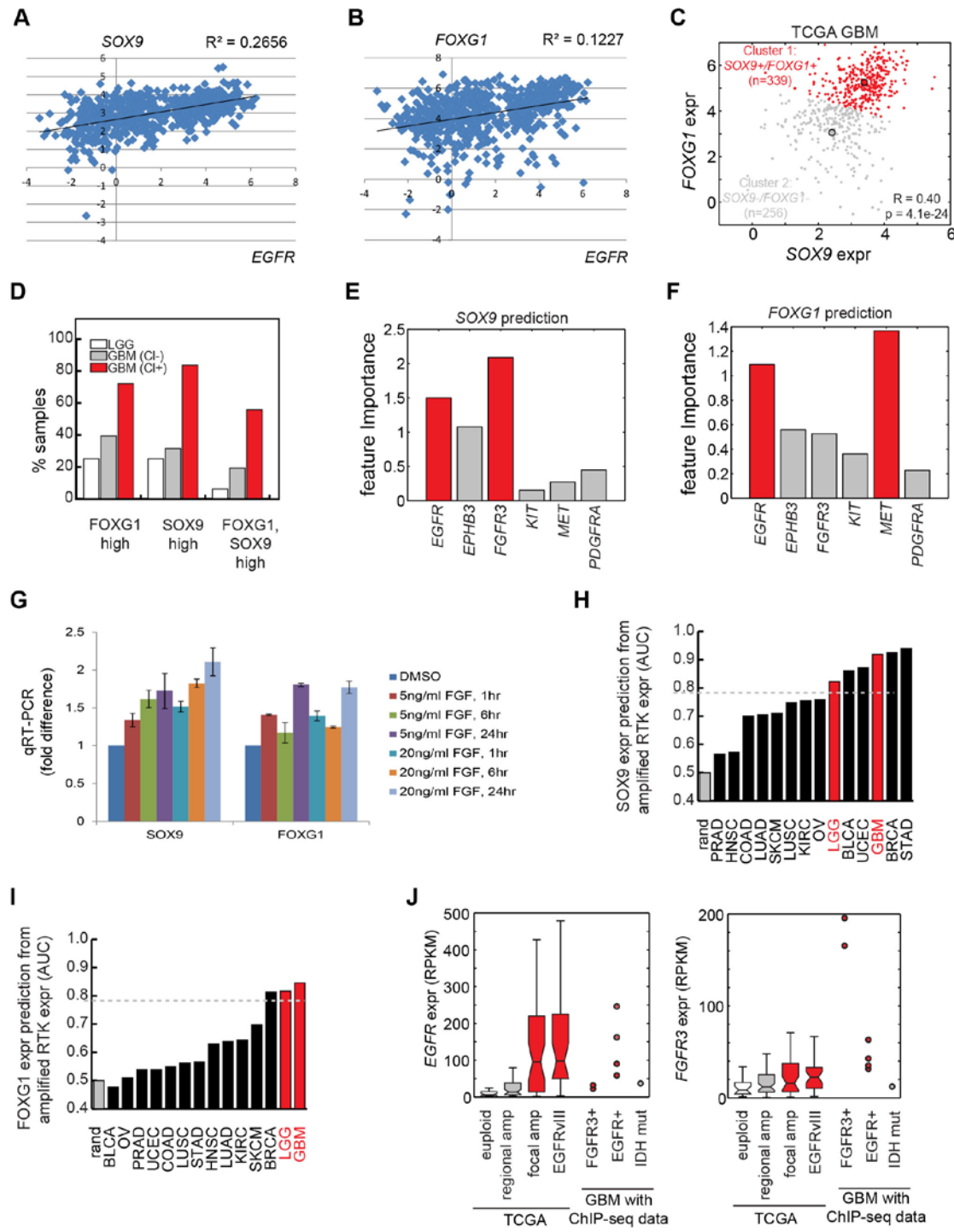


**Figure S4, related to Figure 4.** Correlation of *EGFR* with *SOX9* and *FOGX1* in clinical GBM samples. **(A, B)** Expression levels of *SOX9*, *FOGX1* and *EGFR* in TCGA microarray data of 598 GBM tumors. Each dot represents one tumor. Linear trend line and correlation coefficient ( $R^2$ ) are shown. **(C)** *FOGX1* and *SOX9* are co-expressed at high levels in GBM. **(D)** *FOGX1* and

*SOX9* are expressed at high levels more frequently in the classical subtype (Cl+) of GBM—which are characterized by EGFR amplification and/or mutation—than in non-classical (Cl-) subtype GBMs (the proneural, the neuronal, and the mesenchymal subtypes) and low grade glioma (LGG). (**E, F**) Feature importance of frequently amplified RTKs in predicting the levels of *SOX9* and *FOXG1* in TCGA GBM samples using a random forest classifier. (**G**) Stimulating a U87 cell line overexpressing *FGFR3* with FGF increases the level of *SOX9*, which is consistent with an association between *FGFR3* and *SOX9* in clinical GBM samples. (**H, I**) Summary of experiments using the expression levels of commonly amplified/mutated RTKs (Table S1) to predict the levels of *SOX9* and *FOXG1* in cancers by a random forest classifier. (**J**) Clinical GBM sample information. Tumors in the TCGA GBM database are grouped by the amplification/mutation status of *EGFR*. The genotypes of 7 GBM tumors used in this study for both RNA-seq and ChIP-seq (Figure 4D) are determined by PCR, FISH and ChIP-input DNA sequencing (see Table S2).

See also Table S1.

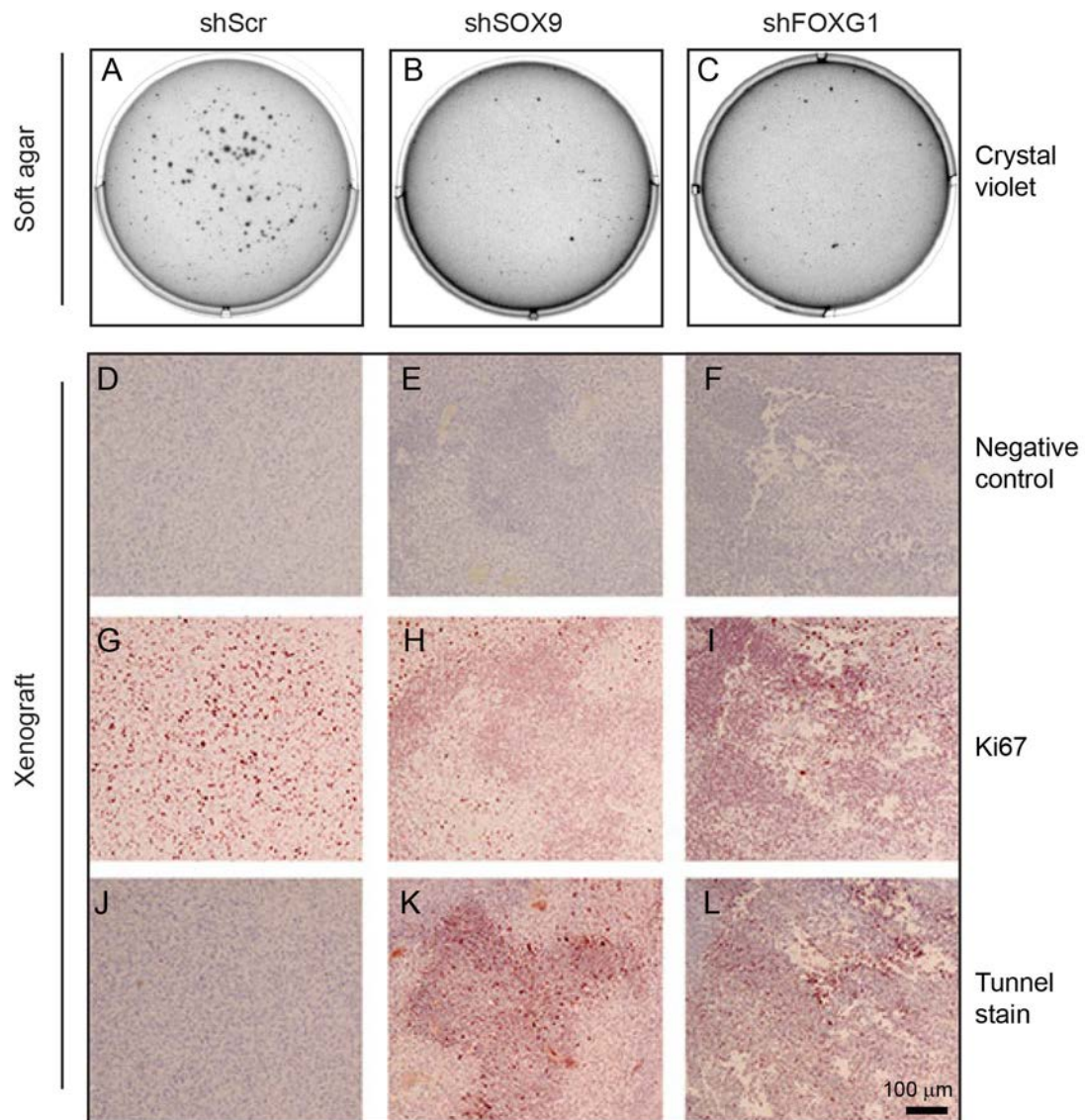


**Figure S5, related to Figure 5.** **(A-C)** Crystal violet stain of U87EGFRvIII cells cultured in suspension in soft agar for 17 days in 6-well culture plates. Knockdown of SOX9 or FOXG1 severely impairs the ability of U87EGFRvIII cells to form large colonies. **(D-L)** Immunohistochemical stain of adjacent sections of the mouse brains that contain intracranially injected U87EGFRvIII cells expressing short hairpin RNAs targeting SOX9, FOXG1, or a scrambled short hairpin RNA sequence. SOX9 and FOXG1 knockdowns both lead to dramatic decrease of Ki67 stain and increase of Tunnel stain in the tumors formed by U87EGFRvIII cells. Scale bar: 100  $\mu$ m.

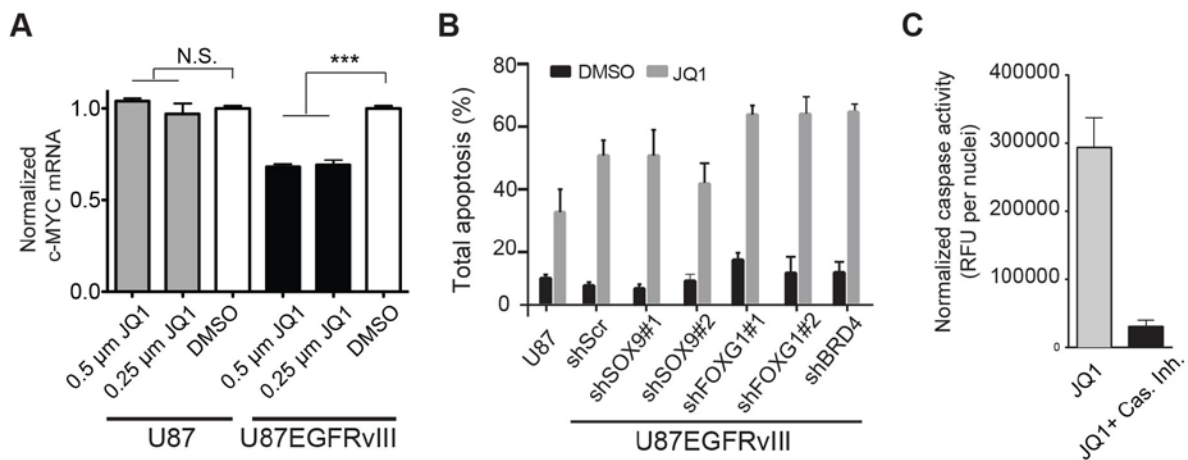


**Figure S6, related to Figure 6. (A)** JQ1 decreases *c-MYC* transcription specifically in U87EGFRvIII cells. qPCR was used to measure *c-MYC* mRNA levels in U87 and U87EGFRvIII cells treated with JQ1 or DMSO for 48 hours. *c-MYC* levels were normalized to both *GAPDH* and *ACTB*, and relative expression was compared to DMSO controls. **(B)** Total apoptosis of DMSO and JQ1 treated U87 and U87EGFRvIII cells, as determined by Annexin V/Propidium Iodide stain. **(C)** Quantitation of live-imaging assay of activated caspases. Incubation of U87 EGFRvIII cells (treated with 1 μM JQ1) with the pan-caspase inhibitor Z-DEVD-FMK (30 μM) immediately prior to staining significantly attenuates the fluorescence signal from the CellEvent reagent ( $p=0.0145$ ).

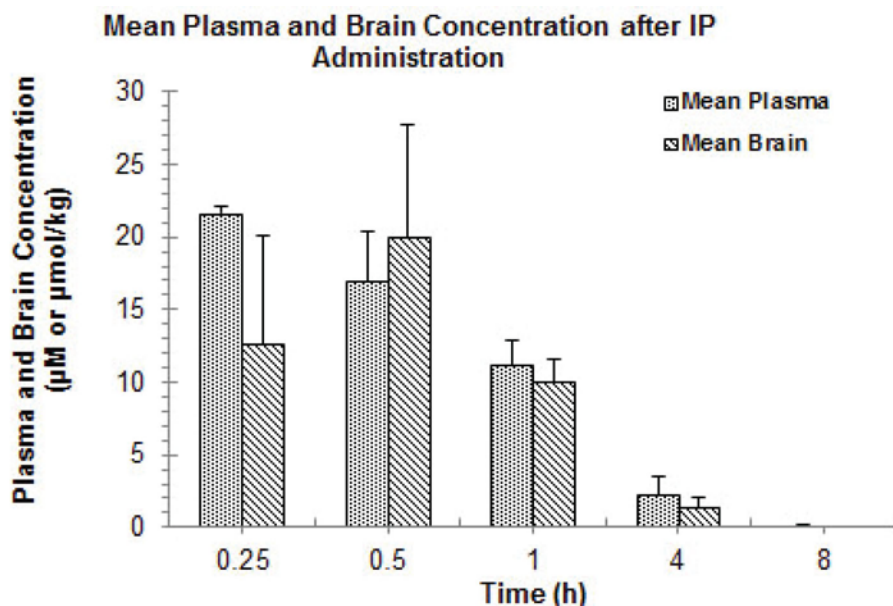


**Figure S7, related to Figure 7.** JQ1 pharmacokinetic profile. Following intraperitoneal injection of JQ1 in female nu/nu mice at 50 mg per kg body weight, drug concentrations in the plasma and the brain were measured by LC/MS at the indicated times. JQ1 exhibited high brain penetration with a maximum brain concentration of ~20  $\mu\text{M}$  at 0.5 hr and a half-life of ~1 hr in both plasma and brain. Experiment was performed by WuXi AppTec, Shanghai, China.

## Supplementary Tables

**Table S1. Related to Figure S4.**

Cancer type	Abbreviation	Frequently amplified receptor tyrosine kinases (RTKs)
Adrenocortical carcinoma	ACC	<i>FGFR3, FGFR4, FLT4</i>
Bladder Urothelial Carcinoma	BLCA	<i>DDR2, EGFR, ERBB2, FGFR1, FGFR3, NTRK1</i>
Breast invasive carcinoma	BRCA	<i>AATK, DDR2, EGFR, EPHB3, ERBB2, FGFR1, FGFR2, IGF1R, NTRK1, NTRK3</i>
Cervical squamous cell carcinoma and endocervical adenocarcinoma	CESC	<i>EGFR, EPHB3, ERBB2, IGF1R</i>
Colon adenocarcinoma	COAD	<i>EGFR, ERBB2, FGFR1, FLT1, FLT3, PTK7</i>
Esophageal carcinoma	ESCA	<i>EGFR, EPHB3, EPHB4, ERBB2, FGFR1, IGF1R, LMTK2, NTRK1, PTK7</i>
Glioblastoma	GBM	<i>EGFR, EPHB3, FGFR3, KDR, KIT, MET, PDGFRA</i>
Head and Neck squamous cell carcinoma	HNSC	<i>EGFR, EPHB3, EPHB4, ERBB2, FGFR1, IGF1R, LMTK2</i>
Kidney renal clear cell carcinoma	KIRC	<i>CSF1R, FGFR4, FLT4, PDGFRB</i>
Brain low grade glioma	LGG	<i>EGFR, EPHA1, EPHB3, IGF1R, KDR, KIT, PDGFRA, STYK1</i>
Liver hepatocellular carcinoma	LIHC	<i>AATK, DDR2, IGF1R, LMTK2, MET, NTRK1, PTK7</i>
Lung adenocarcinoma	LUAD	<i>AATK, DDR2, EGFR, EPHB3, ERBB2, FGFR1, FGFR4, KDR, KIT, MET, NTRK1, PDGFRA, PTK7, TIE1</i>
Lung adenocarcinoma	LUSC	<i>AATK, DDR2, EGFR, EPHA5, EPHA6, EPHB3, EPHB4, ERBB2, FGFR1, IGF1R, KDR, KIT, LMTK2, NTRK1, NTRK3, PDGFRA, TEK</i>
Ovarian serous cystadenocarcinoma	OV	<i>AATK, DDR2, EPHA1, EPHA10, EPHB3, EPHB6, ERBB3, FGFR3, IGF1R, NTRK1, NTRK3, PTK7, TIE1</i>
Pancreatic adenocarcinoma	PAAD	<i>LMTK2</i>

Prostate adenocarcinoma	PRAD	<i>FGFR1, FGFR3</i>
Rectum adenocarcinoma	READ	<i>DDR2, ERBB2, FGFR1, FLT1, FLT3, PTK7</i>
Sarcoma	SARC	<i>DDR2, NTRK1</i>
Skin Cutaneous Melanoma	SKCM	<i>AATK, DDR2, EPHA1, EPHB6FLT4, IGF1R, KIT, NTRK1, NTRK3, PDGFRA</i>
Stomach adenocarcinoma	STAD	<i>DDR2, EGFR, EPHB3, EPHB4, ERBB2, ERBB3, FGFR2, IGF1R, LMTK2, MET, NTRK1, NTRK3, PTK7</i>
Uterine Corpus Endometrial Carcinoma	UCEC	<i>AATK, DDR2, EPHA2, EPHB3, ERBB2, ERBB3, FGFR1, FGFR3, NTRK1, TIE1</i>
Uterine Carcinosarcoma	UCS	<i>AATK, EPHB3, ERBB3, FGFR1, FGFR3, NTRK1</i>

---

\*Frequently amplified RTKs in different cancer types were according to the Broad Institute TCGA Copy Number Portal: <http://www.broadinstitute.org/tcga/home>

**Table S2. Related to Figure 4.**

Tumor ID	Tumor		EGFRviii	EGFR Amplification	IDH1 mutation
	Nuclei	Pathology			
B39	70%	GBM	positive	Yes	Negative
R28	90%	GBM	positive	Yes	Negative
S08	75%	GBM	positive	Yes	Negative
P69	80%	GBM	positive	Yes	Negative
2493	70%	GBM	negative	No	Negative
2585	70%	GBM	negative	No	Negative
IDHmut 5661	70%	Oligoastrocytoma III	negative	No	IDH1 R132H

**Table S3 and Table S4 are Excel spreadsheets attached to this manuscript.**

Table S3: PCR primer sets, related to Figures 2 and 3.

Table S4: ChIP-seq motif analysis, related to Figures 1 and 4.

## **Supplemental Experimental Procedures**

### **Cell Culture**

Cells were cultured at 37 °C in 5% CO<sub>2</sub>, in Dulbecco's Modified Eagle Media (DMEM, Cellgro) supplemented with 10%FBS (Hyclone) and 1% penicillin/streptomycin/glutamine (Invitrogen). Serum-starved cells were obtained by culturing cells in DMEM for 24 hours. For drug treatment *in vitro*, cells were seeded in DMEM+0.5% FBS. DMSO or small compound stocks were added to culture media the next day. Drug used include: erlotinib hydrochloride (Selleck), U0126 (Millipore), torin1 (Selleck). JQ1 (Santai Labs).

### **High Throughput Sequencing Read Mapping**

ChIP-seq experiments were mapped to human genome build hg18 using Bowtie v0.12.5 (Langmead et al., 2009) with the following options: “-v 3 -m 1 --best –strata”. H3K27ac and input ChIP-seq experiments in normal tissue were obtained from the Roadmap Epigenomics Mapping Consortium (GSE17312) and lifted over from hg19 to hg18. PCR duplicates were removed with the Picard tool (<http://broadinstitute.github.io/picard>). Paired-end RNA-seq experiments were mapped using Tophat v1.4.0(Trapnell et al., 2009) with the following parameters: “-g 1 --library-type=fr-firststrand”. 4C-Seq data were mapped using 4Cseqpipe (van de Werken et al., 2012) with the first cutter set as *Nla*III (CATG) and the second cutter set as *Dpn*II (GATC).

### **Enhancer Predictions**

To identify putative enhancers in cell lines with H3K4me1, H3K4me3 and H3K27ac ChIP-seq data, we used RFECS (Rajagopal et al., 2013)to define an initial set and filtered for predictions with at least 1.75-fold enrichment of H3K4me1 or H3K27ac. To identify putative enhancers in tissues and tumor samples with H3K27ac data alone, we used MACS to find H3K27ac peaks (Zhang et al., 2008). Predictions within 5kb of a transcription start site were removed. To identify enhancers specifically active in a set of EGFRvIII positive samples  $P = \{p_1, p_2, \dots\}$  as compared

to a set of EGFRvIII negative samples  $N = \{n_1, n_2, \dots\}$ , we devised the following general strategy. For a given sample  $s$  and histone mark  $h \in H$ , let  $E_{s,h,l}$  denote the enrichment of the histone mark for the sample at locus  $l$  compared to input, as defined above. As the histone marks examined here are enriched as punctuated peaks, we assume that the genome-wide distribution of binned (1kb) data is, to a first approximation, Gaussian. Therefore, the random variables represent the difference between histone modification enrichment between an EGFRvIII+ sample  $p_i$  compared to an EGFRvIII- sample  $n_j$  is  $D_{p_i,n_j,h,l} = E_{p_i,h,l} - E_{n_j,h,l}$ , which is also Gaussian with mean and standard deviation denoted respectively as  $\mu_{p_i-n_j,h}$  and  $\sigma_{p_i-n_j,h}$ . Therefore, the random variable  $G_{p_i,n_j,h,l} = \frac{D_{p_i,n_j,h,l} - \mu_{p_i-n_j,h}}{\sigma_{p_i-n_j,h}}$  follows a Gaussian distribution with mean 0 and variance 1. Finally, let the test statistic  $S_{h,l} = \sum_{p_i \in P} \sum_{n_j \in N} (G_{p_i,n_j,h,l})^2$ , which by definition follows a Chi-squared distribution with degrees of freedom equal to  $|P| \times |N|$ . Higher values of  $S_{h,l}$  indicate increased deviation of samples in  $P$  from samples in  $N$  for locus  $l$ . Since  $S_{h,l}$  is unsigned, we create the indicator random variable  $C_{i,j,h,l} = \begin{cases} 1 & \text{if } G_{p_i,n_j,h,l} > 0 \\ 0 & \text{otherwise} \end{cases}$ . Finally, to identify EGFRvIII-specific enhancers having a histone mark  $h$ , we keep loci  $l$  where  $\sum_i \sum_j C_{i,j,h,l} > C_{cutoff}$  and where the one-sided Chi-Squared p-value for  $S_{h,l}$  is less than  $p_{cutoff}$ , which is determined empirically with randomized data such that  $p_{cutoff}$  corresponds to a false discovery rate of  $F$ . For the cell line comparison of two U87vIII and two U87 samples, we let  $C_{cutoff} = 3$  and  $F = 10\%$ . For the more extensive comparison of six tumor biopsies and seven control specimens, we let  $C_{cutoff} = 0.5 \times |P| \times |N| = 21$  and  $F = 1\%$ .

## Gene Expression Analysis

Total RNA was extracted using the Qiagen RNeasy mini kit (Qiagen). For the quantitative polymerase chain reaction (qPCR) experiments, total RNA was reverse-transcribed to single-stranded cDNA using the SuperScript VILO cDNA synthesis kit (Life Technologies) and qPCR

was performed using the KAPA Sybr green qPCR kit (KAPA Biosystems). For the experiment shown in Figure S6A, total RNA was reverse-transcribed using the High Capacity cDNA Reverse Transcription Kit and qPCR was performed using Taqman Gene Expression Assays (Life Technologies). PCR primer information is shown in Table S3.

### **Western Blot**

Cell lysates were extracted in RIPA buffer. Protein concentrations were determined by the BCA protein assay kit (Thermo Scientific). For Western blots, 20 µg of total protein per sample was electrophoresized in 4-12% gradient SDS-PAGE gel and transferred to PDVL membrane according to Invitrogen protocol (Invitrogen). The membrane was incubated with primary antibodies at 4 °C overnight, followed by incubation with HRP-conjugated secondary antibodies at room temperature for 2 hours. Chemical fluorescence signals were detected by ChemiDoc (Bio-Rad). Antibodies used include rabbit anti-SOX9 (Millipore, Cat#AB5535), rabbit anti-FOXG1 (Active Motif, Cat# 31211), mouse anti- ACTIN (Sigma, Cat# A4700), rabbit anti-EGFR (Millipore, Cat#: 06847MI), rabbit anti-phospho-EGFR Y1068 (Cell Signaling, Cat# 3777S), rabbit anti-ERK1/2 (p44/42) antibody (Cell Signaling, Cat #9102), rabbit anti-phospho-ERK (Thr202/Tyr204) (Cell Signaling, Cat# 9101S), mouse anti-S6 (Cell Signaling, Cat# 2317S), rabbit anti-phospho-S6 (Ser235/236) (Cell Signaling, Cat# 4858S), HRP-linked anti-rabbit IgG antibody (Cell Signaling, Cat#7074S), HRP-linked anti-mouse IgG antibody (Cell Signaling, Cat# 7076S). All antibodies were diluted 1-2,000, except that the mouse anti-Actin antibody was diluted 1:10,000.

### **Immunohistochemistry**

Formalin-fixed, paraffin-embedded (FFPE) tissue sections were prepared by the Histology Core Facility at UCSD Moores Cancer Center. Immunohistochemistry was performed according to standard procedures. Antigen was retrieved by boiling slides in 0.01 M of sodium citrate (pH 6.0) in a microwave for 15 min. Sections were incubated with primary antibodies at 4 °C

overnight, followed by incubation with biotinylated secondary antibodies at room temperature for 30 min. Antibodies used include: rabbit anti-SOX9 (Millipore, Cat# AB5535), rabbit anti-FOXG1 (Thermo Scientific, Cat# PA5-26794), anti-Ki67 (Thermo Scientific, Cat# PA5-16785). phospho-PDGFRbeta (Y751) (Cell Signaling, Cat# 3161L), and phospho-Met (Y1234/1235) (Cell Signaling, Cat# 3077P). All antibodies were used in 1:200 ~1:500 dilutions.

### **Plasmid Constructs**

The infra-Red Fluorescent Protein 720 (iRFP720) Cdna (Shcherbakova and Verkhusha, 2013) was PCR-cloned into the *Nhe* I and *Xho* I restriction enzyme sites of the lentiviral plasmid vector pLV. Short hairpin constructs were purchased from Sigma: shSOX9#1 (TRC#: TRCN0000020384; target sequence: 5'-GCATCCTCAATTCTGTA-3'), shSOX9#2 (TRC#: TRCN0000020386 ; target sequence: 5'-CTCCACCTTCACCTACATG-3'), shFOXG1#1 (TRC#: TRCN0000013952; target sequence: 5'-CATGAAGAACTTCCCTAC-3'), shFOXG1#2 (TRC#: TRCN0000013949; target sequence: 5'-CCACAATCTGTCCCTAAC-3'). shBRD4 (TRC#: TRCN0000196576; target sequence: 5'-GCCAAATGTCTACACAGTA-3').

### **Lentivirus Production and Infection**

Lentiviral plasmid constructs were co-transfected with lentivirus packaging plasmids to Lenti-X 293T cells (Clontech), using X-tremeGENE DNA transfection reagents (Roche). Supernatants containing high titer lentiviruses were collected between 24-72 hours after transfection and were filtered through a 0.45  $\mu$ m syringe filter before use. For infection experiments,  $5 \times 10^5$  U87 and U87EGFRvIII cells were seeded in 10 cm culture dish. On the next day, 1/10 volume of high titer lentivirus and 12.5 ng/ml (final concentration) of polybrene were mixed and added to cultured cells. After 8 hours of incubation in 37 °C, the supernatant containing virus was replaced by fresh culture media (DMEM/10%FBS). Infected cells were selected by puromycin (1  $\mu$ g /ml) or blasticidin (2  $\mu$ g /ml).

## **siRNA Transfection**

Transient knockdown experiments using siRNA was performed as described (Akhavan et al., 2013). siRNAs were purchased from Life Technologies. siEGFR#1 (Ambion Silencer Select ID: s564). siEGFR#2 (Ambion Silencer Select ID: s565).

## **Caspase Assay**

Cells (2000/well for U87 and U87 EGFRvIII kinase dead, 1500/well for U87 EGFRvIII) were seeded in optical 96-well plates (Greiner, 655090) and incubated for 16 hours at 37°C, 5% CO<sub>2</sub>. JQ1 (DMSO stock; dose response from 0.03 µM to 10 µM) and 4 µM CellEvent Caspase-3/7 Green Reagent (Life Technologies, C10423) were then added to the culture medium. After 96 hours at 37°C, 5% CO<sub>2</sub>, NucBlue Live ReadyProbes Reagent (Hoechst 33342; Life Technologies, R37605) was added 30 minutes prior to imaging on a Cell Voyager 7000 spinning disk confocal imaging system (Yokogawa Electric Corporation) with a 20X 0.75 NA U-PlanApo objective and 2560x2160 sCMOS camera (Andor) at 2x2 binning. The imaging chamber was maintained at 37°C and 5% CO<sub>2</sub>. Image acquisition and data analysis were performed using the CV7000 software. 6-8 fields/well were imaged, with duplicate wells for each condition. 3 x 2 µm z-sections in the blue (40 % power, 300 ms, 2.2X gain) and green (40 % power, 300 ms, 2.2X gain) channels were captured in each field. JQ1-dependent caspase activity per cell was calculated by dividing the total fluorescence at 530 nm (corresponding to the cleaved caspase reporter reagent) by the number of nuclei (Hoechst staining) and then subtracting background fluorescence per cell (as determined from the DMSO-treated wells). EC<sub>50</sub>s were computed using this normalized data and a 4-parameter, variable slope fit with Prism 5 (GraphPad). In control studies (Figure S6B), cells were plated as above. After 16 hours at 37°C, 5% CO<sub>2</sub>, JQ1 (1 µM) was added to the culture medium. After an additional 96 hours at 37°C, 5% CO<sub>2</sub>, the cells were treated with 30 µM Z-DEVD-FMK (Tocris) for 1 hour prior to staining with the CellEvent Caspase 3/7 Green and NucBlue Live ReadyProbes Reagents for 1 hour. Imaging

and data analysis were performed as above.

### **Cell Proliferation and Viability Assay**

Cells were seeded in 12-well culture plates at 15,000 cells per well. After three days, total and live cells in each well were counted by Trypan blue assay using a TC10 automatic cell counter (Bio-Rad).

### **Flow Cytometry**

Cells were seeded at a density of 37,500 in each well of 6-well plate. The following day, DMSO or 1  $\mu$ M JQ1 was added in DMEM media containing 2.5% FBS. Annexin V/Propidium Iodide (PI) staining was carried out 5 days following JQ1 treatment using the FITC Annexin V Apoptosis Detection Kit II (BD Biosciences). Flow cytometric analyses were performed using the BD LSR II Flow Cytometer System (BD Biosciences). 10,000 cells within the gated population were analyzed.

### **Supplemental References**

- Akhavan, D., Pourzia, A.L., Nourian, A.A., Williams, K.J., Nathanson, D., Babic, I., Villa, G.R., Tanaka, K., Nael, A., Yang, H., *et al.* (2013). De-repression of PDGFRbeta transcription promotes acquired resistance to EGFR tyrosine kinase inhibitors in glioblastoma patients. *Cancer discovery* 3, 534-547.
- Langmead, B., Trapnell, C., Pop, M., and Salzberg, S.L. (2009). Ultrafast and memory-efficient alignment of short DNA sequences to the human genome. *Genome biology* 10, R25.
- Rajagopal, N., Xie, W., Li, Y., Wagner, U., Wang, W., Stamatoyannopoulos, J., Ernst, J., Kellis, M., and Ren, B. (2013). RFECs: a random-forest based algorithm for enhancer identification from chromatin state. *PLoS computational biology* 9, e1002968.

- Shcherbakova, D.M., and Verkhusha, V.V. (2013). Near-infrared fluorescent proteins for multicolor *in vivo* imaging. *Nature methods* 10, 751-754.
- Trapnell, C., Pachter, L., and Salzberg, S.L. (2009). TopHat: discovering splice junctions with RNA-Seq. *Bioinformatics* 25, 1105-1111.
- van de Werken, H.J., Landan, G., Holwerda, S.J., Hoichman, M., Klous, P., Chachik, R., Splinter, E., Valdes-Quezada, C., Oz, Y., Bouwman, B.A., *et al.* (2012). Robust 4C-seq data analysis to screen for regulatory DNA interactions. *Nature methods* 9, 969-972.
- Zhang, Y., Liu, T., Meyer, C.A., Eeckhoute, J., Johnson, D.S., Bernstein, B.E., Nusbaum, C., Myers, R.M., Brown, M., Li, W., *et al.* (2008). Model-based analysis of ChIP-Seq (MACS). *Genome biology* 9, R137.